Mitochondrial translation is required for sustained killing by cytotoxic T cells‡

Authors: Miriam Lisci[1], Philippa R. Barton[1], Lyra O. Randzavola[1,†], Claire Y. Ma[1], Julia M. Marchingo[2], Doreen A. Cantrell[2], Vincent Paupe[3], Julien Prudent[3], Jane C. Stinchcombe[1], Gillian M. Griffiths[1,*]

Affiliations:
[1]Cambridge Institute for Medical Research, University of Cambridge, Cambridge Biomedical Campus, CB2 0XY, UK.
[2]Cell Signalling and Immunology Division, School of Life Sciences, University of Dundee, Dundee DD1 5EH, UK.
[3]MRC Mitochondrial Biology Unit, University of Cambridge, Cambridge Biomedical Campus, CB2 0XY, UK.
[†]Current address: Department of Immunology and Inflammation, Imperial College London, W12 0NN, UK.
[*]Corresponding author: gg305@cam.ac.uk

Abstract: T cell receptor activation of naïve $CD8^+$ T lymphocytes initiates their maturation into effector cytotoxic T lymphocytes (CTLs) which can kill cancer and virally infected cells. Although CTLs show an increased reliance on glycolysis upon acquisition of effector function, we found an essential requirement for mitochondria in target cell killing. Acute mitochondrial depletion in USP30-deficient CTLs markedly diminished killing capacity although motility, signaling, and secretion were all intact. Unexpectedly, the mitochondrial requirement was linked to mitochondrial translation, inhibition of which impaired CTL killing. Impaired mitochondrial translation triggered attenuated cytosolic translation, precluded replenishment of secreted killing effectors, and reduced the capacity of CTLs to carry out sustained killing. Thus, mitochondria emerge as a previously unappreciated homeostatic regulator of protein translation required for serial CTL killing.

One-Sentence Summary: Mitochondria are homeostatic regulators of serial killing by cytotoxic T lymphocytes.

Main Text:

$CD8^+$ cytotoxic T lymphocytes (CTLs) are key players of the adaptive immune response. Activation of T cell receptors (TCRs) on naïve $CD8^+$ T cells converts them into effector CTLs able to kill tumorigenic and virally infected cells. CTLs initiate cell death by secreting cytotoxic proteins, including perforin and granzymes, which selectively trigger caspase activation and subsequent apoptosis (*1*). An important attribute of CTLs is their ability to carry out "serial killing", with a single CTL attacking multiple targets one after another, facilitating sustained killing (*2-4*). Thus, CTL function relies on motility to find and engage targets, TCR signaling for activation, and regulated secretion to effect killing.

Mitochondria play crucial roles in the adaptive immune system, mediating the development, metabolism, and activation of T cells (*5-7*). Although mitochondrial mass is correlated with CTL anti-tumor activity and increases after TCR-mediated activation (*8-10*), paradoxically CTLs show enhanced aerobic glycolysis (*11, 12*). How or why mitochondria impact target cell killing by differentiated CTLs is not well understood.

The removal of mitochondria by autophagy (mitophagy) is an important contributor to mitochondrial abundance and quality control (*13, 14*). The autophagic machinery can be recruited to mitochondria via a ubiquitin coat that forms in response to mitochondrial stress. Promiscuous ubiquitination is thought to be minimized by USP30, a transmembrane deubiquitinase (DUB) localized on the outer mitochondrial membrane (*15-17*). Thus, the loss of USP30-mediated deubiquitination results in increased mitophagy, thereby reducing cellular mitochondrial content.

A large-scale screen of single-gene deletion mice for immunological function identified USP30 as a regulator of CTL killing (*18*). T cell development was normal in *Usp30*$^{-/-}$ (KO) mice but CTLs generated after activation of naïve $CD8^+$ T cells showed reduced killing of target cells. The role of USP30, and by inference mitochondria, in CTL function was intriguing

because there is an increased reliance on glycolysis in activated effector T cells (*11*). These observations raised the possibility that mitochondria play a previously unappreciated role in CTL biology, and pointed to USP30 as a starting point for investigating this connection.

Results

Activation leads to an acute loss of mitochondria in USP30-deficient CD8$^+$ T cells

T cell development was unaffected in KO mice (*18*), with normal T cell populations in the spleen (fig. S1) that could then be used to generate CTLs, acquiring cytolytic activity 5-7 days after activation (Fig. 1A). Using tetramethylrhodamine ethyl ester (TMRE) (Fig. 1B) and MitoTracker Green (Fig. 1C) to label mitochondrial membrane potential and mass, respectively, we noted that WT and KO signals overlapped prior to activation (day 0). Upon activation, both WT and KO signals increased by day 3, consistent with an increase in mitochondria in activated T cells (*9*, *10*). However, by days 5-7, there was a loss of signal in KO but not WT CTLs, suggesting that mitochondria were selectively impacted in KO CTLs after TCR activation. Using immunofluorescence microscopy, we found that by day 5 after activation KO CTLs showed reduced levels of both the mitochondrial outer membrane protein TOM20 as well as the mitochondrial matrix enzyme pyruvate dehydrogenase (PDH) compared to WT CTLs (Fig. 1, D and E, and fig. S2). Using transmission electron microscopy (TEM), mitochondria in day 5 KO CTLs exhibited absent or disorganized cristae, with an empty appearance compared with mitochondria in WT CTLs (Fig. 1F), consistent with a role for USP30 in safeguarding the mitochondrial import protein TOM20 (*19*). Quantitation of TEM images demonstrated that 32% of KO CTLs showed disrupted mitochondrial morphology, whereas 60% lacked mitochondria completely. Only 8% of KO CTLs showed normal mitochondrial morphology compared with 73% of WT CTLs (Fig. 1G). Furthermore, the fluorescent, pH-dependent mitochondrial-Keima mitophagy reporter (mt-Keima) (*20*) revealed

an increased mitophagic signal (red) in KO CTLs. Thus, TCR activation of $CD8^+$ T cells lacking USP30 appeared to induce significant changes in mitochondrial number and morphology (Fig. 1, H and I, and movies S1 and S2).

Given the altered mitochondrial morphology, we asked whether mitochondrial function was affected. Oxidative phosphorylation was markedly reduced in day 5 KO CTLs, showing significant differences between both basal and maximal rates of respiration compared to WT CTLs (Fig 1J). Moreover, the decrease in oxygen consumption rate (OCR) was accompanied by an increase in extracellular acidification rate (ECAR), suggesting an even greater reliance on glycolysis in KO compared to WT CTLs (Fig. 1K). Thus, activation of $CD8^+$ T cells lacking USP30 results in the generation of CTLs with significant changes in mitochondrial number and morphology, which are associated with impaired function.

Mitochondrial depletion inhibits killing

We found that day 5 KO CTLs exhibited a reduced killing capacity, particularly when required to kill for extended periods or when the number of CTLs was limiting. In a short-term killing assay, KO CTLs failed to kill targets until the ratio of CTL to targets was >7 and only killed 40% of target cells when CTLs outnumbered targets by 25:1. By contrast, WT CTLs killed targets within 2.5 hours when the ratio of CTL to targets was >1 and killed all targets when CTLs outnumbered targets by 25:1 (Fig. 2A). Furthermore, a longer-term assay with 10 CTLs per target showed that KO CTLs took almost twice as long as WT CTLs to kill all targets (Fig. 2B), demonstrating a reduced killing capacity in KO CTLs. Reducing the number of CTLs per target to 1:1 revealed similar levels of killing for WT and KO CTLs over the first 4 hours, after which KO CTLs showed no further killing, suggesting that KO CTLs lost the capacity to kill over time (Fig. 2C).

ATP production, motility, signaling and secretion are unaffected by loss of mitochondria

Mitochondria could contribute to many of the different steps required for killing as CTL seek, recognize, and kill their targets. Therefore, we sought to identify which were impacted in KO CTLs. First we asked whether reduced oxidative phosphorylation affected killing by testing day 5 CTLs from *Ndufs4*$^{-/-}$ mice in which complex I was disrupted (*21*). Despite a defect in maximal mitochondrial respiration, there was no defect in T cell development in *Ndufs4*$^{-/-}$ mice (fig. S3) or in CTL killing using either this genetic model, inhibitors of complex I, III, and V, or disruption of mitochondrial membrane potential (Fig. 2, D to F). As mitochondrial ATP has been shown to play a role in lymphocyte migration (*22*), we asked whether motility or ATP levels were affected in day 5 KO CTLs. We found no difference in motility (Fig. 3A and movies S3 and S4) nor overall ATP concentrations between WT and KO CTLs, with ATP concentrations reduced in both WT and KO upon selective inhibition of oxidative phosphorylation (oligomycin) or glycolysis (2-deoxy-D-glucose (2-DG)) (Fig. 3B). We found no defect in conjugate formation between day 5 KO CTLs and target cells or in polarization of the centrosome or cytolytic granules to the synapse formed between CTLs and targets (Fig. 3, C and D). Furthermore, day 5 KO CTLs showed no defects in either TCR-stimulated calcium fluxes nor the release of granules in response to TCR activation (Fig. 3, E and F). Proximal and distal signaling events driven by TCR engagement also showed no difference between day 5 WT and KO CTLs (fig. S4). Thus, ATP levels, motility, polarization, signaling, and secretion were all unaffected in KO CTLs.

Mitochondrial depletion leads to translation attenuation and loss of cytolytic proteins

Given that all steps to secretion appeared to be intact, we asked whether the secretory granules that store the cytolytic proteins required for killing were affected in day 5 KO CTLs. There were no gross changes in the morphology of KO compared to WT granules. However, we did

note that although similar in number, the granules were smaller (quantitated by reduced surface area) in KO CTLs (Fig. 4, A to C). There was no evidence of granule autophagy, suggesting that the reduced size might rather reflect a reduction in granule content. Two of the key cytolytic proteins stored in granules are granzyme B and the pore-forming protein perforin (*1*). Granzyme B expression in KO CTLs was reduced relative to WT at days 5 and 7 after activation (Fig. 4D). Furthermore, although perforin was rapidly processed to its mature active form in WT CTLs, incompletely processed forms were evident in day 5 KO CTLs with a reduced level of mature perforin (Fig. 4E) (*23*). Notably, loss of protein was not due to changes in transcription, as mRNA expression was unchanged in day 5 KO relative to WT CTLs (Fig. 4F), suggesting that a defect in protein synthesis may underlie the loss of cytolytic proteins in the KO.

Protein synthesis, monitored by incorporation of the methionine analogue homopropargylglycine (HPG) (*24*), was markedly reduced in day 5 KO CTLs relative to WT (Fig. 4G). Mimicking target encounter by cross-linking TCR (using anti-CD3ε) led to a modest increase in protein synthesis. This included renewed synthesis of granzyme B and perforin with newly synthesized intermediates of higher molecular weight (*25*), appearing in day 5 WT CTLs that could be abolished by treatment with the cytosolic protein synthesis inhibitor cycloheximide (CHX) (Fig. 4, H and I). By contrast, new synthesis was much reduced in the KO, suggesting that a defect in mRNA translation of cytolytic proteins might cause the loss of killing observed in KO CTLs. To test this, we treated day 5 WT and KO CTLs with CHX in a long-term killing assay that required sustained killing. WT CTLs killed for the first 4 hours, after which CHX treatment reduced cytotoxicity, mirroring the pattern of killing by KO CTLs (Fig. 4J). In KO CTLs treated with CHX, target cell killing showed a further decrease between 2-8 hours, consistent with the low levels of cytosolic protein synthesis observed. Thus, de novo protein synthesis is required for sustained CTL killing and is impaired in KO CTLs.

Cytolytic proteins are selectively impacted by the translational defect in USP30-deficient CTLs

To determine whether the translational defect impacted all proteins equally, we used mass spectrometry to compare the proteomes of day 5 WT and KO CTLs before and after TCR activation. Mass spectrometry data was normalized to the number of cells using a histone ruler approach in order to estimate protein mass and copy number per cell. Analysis of these data not only confirmed the absence of USP30 (table S1), but also revealed that the decrease in protein synthesis did not affect the abundance of all proteins equally. Only a subset of proteins (557) was found to have a significantly lower expression in KO CTLs (fold change>2, FDR<10%) (Fig. 5A to C). Most affected were mitochondrial proteins (72%) (Fig. 5, B and C, and table S1), presumably reflecting their degradation by promiscuous mitophagy in the absence of USP30. Other highly downregulated proteins included granzyme B and eomesodermin, a transcription factor that regulates expression of cytotoxic proteins including perforin, granzyme B, and interferon gamma (IFN-γ) (*26*) (Fig. 5B and table S1). A smaller number of proteins (35) were found to be significantly upregulated in KO CTLs (fold change>2, FDR<10%), including 11 proteins encoded from genes linked to the integrated stress response (*Cebpb, Hmox1, Avil, Bcl2l11, Slca9, Niban1, Ifrd1, Cth, Bbc3, Ca2*, and *Plin2*) and one involved in autophagy (*p62/Sqstm1*) (Fig. 5B and table S1). Upon TCR activation of CTLs, additional cytolytic proteins were downregulated in KO CTLs (Fig. 5D and table S2), including IFNγ, TNFα, and TNFβ (Fig. 5E, fig. S5, and table S2). Thus, in addition to the loss of mitochondrial proteins, cytolytic proteins were particularly affected, decreasing the ability of KO CTLs to mount an effective response. Mitochondrial ribosomal proteins represented one of the most downregulated subsets within the mitochondrial compartment both before and after TCR stimulation (Fig. 5F). Cytosolic ribosomes were unaffected, indicating that the translation

attenuation observed in the KO CTLs was not caused by a defect in cytosolic ribosomal content (Fig. 5G). Thus, mitochondria may be modulating the killing capacity of CTLs by regulating levels of cytolytic proteins.

Mitochondrial translation is required for sustained CTL killing

It is now well established that mitochondrial translation can regulate the synthesis of cytosolic proteins (*27, 28*). In addition, recent in vivo studies suggest roles for mitochondrial translation in T cell function (*29, 30*). We therefore asked whether mitochondrial protein synthesis was disrupted in day 5 KO CTLs by examining HPG incorporation when cytosolic translation was inhibited by CHX (Fig. 6A) (*31*). Mitochondrial translation was evident in WT CTLs with HPG colocalizing with the mitochondrial marker, PDH. By contrast, there was little HPG incorporation in KO CTLs (Fig. 6A). To directly address the role of mitochondrial protein translation in CTL killing, we disrupted mitochondrial protein translation pharmacologically using doxycycline (DOX) (Fig. 6). DOX treatment inhibited CTL cytotoxicity after 4 hours, which replicated the phenotype of KO CTL. There was a small additive effect of DOX treatment in KO CTLs, consistent with the inhibition of any remaining mitochondria in KO CTLs (Fig. 6B). Furthermore, cytosolic protein translation was inhibited after 1 hour of DOX treatment (Fig. 6C) and de novo synthesis of granzyme B and perforin after TCR activation (4 hours) was also reduced (Fig. 6 D and E). These results were recapitulated with chloramphenicol inhibition of mitochondrial protein synthesis (fig. S6). Thus, the selective inhibition of mitochondrial translation is sufficient to attenuate selective cytosolic protein translation and to impair CTL cytotoxicity.

Discussion

Inhibition of mitochondrial translation is known to affect cytosolic translation via several pathways, including mTOR and the integrated stress response (ISR) (*27, 28*). However, these pathways do not appear to be causative in the mitochondrial regulation of CTL killing. The mTOR target and ribosomal protein, S6, was phosphorylated in both KO and WT CTLs (fig. S4). In addition, although we identified upregulation of some ISR proteins in KO CTLs, the ISR inhibitor (ISRIB) only partially restored protein synthesis and was unable to restore killing in KO CTLs (fig. S7). Two distinctive features of the KO CTLs were decreased oxidative phosphorylation (and increased reliance on glycolysis) (Fig. 1, J and K) together with selectivity in the downregulation of cytosolic protein synthesis (Fig. 5). Our proteomic analyses suggested an alternative mechanism that may contribute to the loss of killing when mitochondrial disruption triggers changes in metabolic pathways in the cell. Many metabolic enzymes can "moonlight" as RNA-binding proteins (RBPs), which regulate the translation of selected mRNAs (*32*). The moonlighting functions of RBP metabolic enzymes can be induced by changes in CTL metabolism and can regulate expression of cytolytic proteins including granzyme B, TNFα, and IFNγ (*33-35*). There was a selective downregulation of proteins in KO CTLs compared to CHX-treated CTLs (fig. S8A, and tables S1 and S3). Moreover, the expression of RBP enzymes was altered in both KO CTLs and CTLs where mitochondrial translation was inhibited (fig. S8, B to D, and tables S1 and S4). Using GO enrichment analysis, we noted 68% of commonly downregulated proteins in KO and DOX-treated CTLs were involved in cellular metabolism. We propose that this metabolic re-wiring leads to the selective decrease in proteins required for sustained killing when mitochondrial translation is impaired.

Our study highlights a role for mitochondria as homeostatic regulators of CTL killing. Early in an immune response antigen-specific CTLs will be limiting and the ability of individual CTLs to carry out sustained, serial killing will be critical to the success of the response. Although previous studies have shown that the translational landscape of $CD8^+$ T

cells is especially active as they proliferate and acquire effector capacity (*24*), we now find that de novo protein synthesis is also required to sustain ongoing killing. Given the high energy demands required for protein synthesis (*36*), CTLs that need to continue killing have to rapidly rebalance their overall energy needs. We find that this is mediated by mitochondria with the production of new cytolytic proteins synchronized with mitochondrial translation. In this way, mitochondria act as homeostatic regulators in times of high metabolic demand and serve a crucial function in sustained CTL killing.

Materials and Methods

(Reagents used in this study are listed in Table S5)

Mice

WT C57BL/6N and *Usp30*$^{-/-}$ (Usp30^{tm2b}(EUCOMM)^{Hmgu}) mice were bred and housed in the University of Cambridge Facility. This research has been regulated under the Animals (Scientific Procedures) Act 1986 Amendment Regulations 2012 following ethical review by the University of Cambridge Animal Welfare and Ethical Review Body (AWERB). Age-matched animals (male and female) of 8-20 weeks of age were used in experiments. Spleens from *Ndufs4*$^{-/-}$ mice were supplied by C.Viscomi and M. Zeviani (University of Padua) from mice at 4 weeks of age.

Cell culture, and mitochondrial inhibitors

Single-cell suspension of splenocytes, isolated using 70-µm cell strainers, were activated on plates coated with 0.5 µg/ml of anti-mouse CD3ε and 1 µg/ml of CD28 in CTL culture medium (RPMI 1640, 10% FBS, 2 mM glutamine, 1 mM sodium pyruvate, 100 U/ml of penicillin, 1 mg/ml of streptomycin, 50 µM β-mercaptoethanol, and 100 U/ml of mouse IL-2) for 48 hours at 37°C. After 72 hours CD8$^+$ T cells were purified following manufacturer's instructions for the CD8a$^+$ T Cell Isolation Kit and cultured in CTL medium. P815 and P815-blue (*37*) target cells were grown in DMEM, 10% FBS, penicillin-streptomycin. P815-NucLight transduced cells (*38*) were maintained under 1 µg/ml puromycin selection.

Mitochondrial translation was inhibited by supplementing the cell culture media with 10 µg/ml of doxycycline or 50-500 µg/ml of chloramphenicol throughout the killing (12 hours) and translation (1 hour) assays. CTLs used for immunoblots were treated with 10 µg/ml of doxycycline or 500 µg/ml of chloramphenicol for 4.5 hours before cell lysis. The integrated stress response was inhibited using 100 nM ISRIB throughout killing and translation assays.

Mitochondrial respiration was inhibited in the Mito Stress (Seahorse) and killing (IncuCyte) assays using 1 μM FCCP, 1 μM oligomycin A, 0.5 μM rotenone, and 0.5 μM antimycin A.

Killing assays

CTLs (5 days after activation) were plated at the CTL-to-target ratios shown in phenol red-free RPMI 1640 (2% FBS, 1% penicillin, and streptomycin) in round-bottomed 96-well plates with 10^4 P815 per well in the presence of 1 μg/ml of anti-mouse CD3ε. Cultures were then incubated at 37°C, 10% CO_2 for 2.5 hours (short-term killing). The percentage of target cell lysis was determined using the CytoTox 96 assay following manufacturer's instructions.

Long-term killing assays were imaged in the IncuCyte S3 Live Cell Analysis System (Sartorius) that contains a Basler Ace 1920-155um compact camera and 4X objective, resolution 2.82 microns/pixel. CTLs (5 days after activation) were mixed with P815-NucLight targets in CTL culture medium with 1 μg/ml of anti-mouse CD3ε at the CTL-to-target ratios shown in ultra-low attachment round-bottomed 96-well plates (Corning, 7007). Plates were scanned using a 4X objective lens in both the brightfield and red (excitation: 655 nm; emission: 681 nm) channels and analyzed using IncuCyte S3 v2018b software (Sartorius) to determine loss of target cells over time based on decrease of red fluorescence intensity.

Granule release assay

CTLs (5 days after activation) were incubated with anti-CD107a-PE (LAMP1) in CTL culture medium in the presence or absence of P815 target cells with 1 μg/ml of anti-mouse CD3ε for 2.5 hours at 37°C, 10% CO_2. Cells were resuspended in ice-cold FACS buffer (PBS, 10% FBS), labeled for 20 min at 4°C with Brilliant Violet 711-conjugated anti-CD8 and Zombie Yellow, washed, and analyzed on an Attune NxT (ThermoFisher).

Calcium flux assay

CTLs (5 days after activation) were incubated with 1 μM INDO-1 for 30 min at 37°C, washed and incubated with 1 μg/ml of APC-conjugated anti-CD8 and 5 μg/ml of anti-CD3ε for 15 min

at room temperature. CTLs were resuspended in T cell media and basal INDO-1 MFI was recorded for 1 min on an LSR Fortessa (Becton Dickinson). INDO-1 was excited at 355 nm and emission was collected at 450 nm (Ca^{2+}-unbound) and at 379 nm (Ca^{2+}-bound). TCR was crosslinked by addition of 50 μg/ml of goat anti-hamster antibodies and subsequent calcium fluxes were recorded for 5 min, after which 1 μg/ml of ionomycin was added to determine maximal calcium flux for 2 min. The MFI ratio of Ca^{2+}-bound to Ca^{2+}-unbound INDO-1 (379/450) was calculated to display changes in intracellular calcium concentration.

SDS-PAGE and immunoblotting

Cells were lysed in RIPA buffer (50 mM Tris HCl pH 8.0, 150 mM NaCl, 1% NP-40, 0.5% sodium deoxycholate, and 0.1% SDS) at 2×10^7 cells/ml. Lysates were resolved using 4 to 12% Bis-Tris or 7.5% SDS gels for perforin, before transfer to nitrocellulose filters. Membranes were blocked in 5% milk or 5% BSA (as indicated by antibody manufacturer) for 1 hour at room temperature before overnight incubation at 4°C with primary antibodies against β-actin, calnexin, granzyme B, perforin, TOM20, or phospho-S6 (Ser240/244). Membranes were washed in PBS, 0.1% Tween, incubated with goat anti-rabbit, mouse or rat HRP-conjugated antibodies for 1 hour in 5% milk or 5% BSA before washing and developing using ECL prime detection reagents (GE Healthcare, RPN2232) and imaged using a ChemiDoc MP Imaging System (Bio-Rad).

RNA extraction and real-time qPCR

Total RNA was extracted from CTLs (5 days after activation) using the RNeasy mini kit and QIAshredder columns and 100 ng per sample was used to synthesize cDNA using the Accuscript high fidelity first strand cDNA synthesis kit. Granzyme B and perforin gene expression were measured using the TaqMan Gene Expression Assay with qPCR probes for mouse transcripts of granzyme B, perforin, and TATA-binding protein (Tbp) as a control, using

the 7500 Real-Time PCR System (ThermoFisher). mRNA abundance was quantified by calculating the C_T of the target of interest and normalizing to Tbp (ΔC_T).

Measurement of mitochondrial mass and membrane potential

Mouse CTLs were labeled with Zombie Yellow and Brilliant Violet 711-conjugated anti-CD8a for 15 min at room temperature, washed, and then incubated with 100 nM MitoTracker Green and 100 nM TMRE for 30 min at 37°C, 10% CO_2. Samples were analyzed on day 0 (naïve T cells) and days 3, 5, and 7 post activation using an LSR Fortessa.

Immunofluorescence imaging

CTLs (5 days after activation) were washed in serum-free RPMI 1640 and allowed to adhere to slides at 37°C, 10% CO_2 for 10 min before fixation with 5% paraformaldehyde (PFA) for 15 min at 37°C and quenching in 50 mM ammonium chloride at room temperature. Cells were permeabilized for 10 min in either 0.1% Triton X-100 for PDH staining, or 0.1% saponin for TOM20 staining and blocked using PBS, 1% BSA for PDH staining, or 1% BSA, 0.1% saponin for TOM20 staining. Cells were labeled using anti-TOM20 or PDH for 2 hours washed in PBS, 1% BSA (PDH) or PBS, 1% BSA, 0.1% saponin (TOM20), incubated with goat anti-mouse Alexa Fluor (AF) 546 for 1 hour, washed in PBS, Hoechst 33342 and mounted in ProLong Diamond. Samples were imaged using a Zeiss 63X 1.4NA PlanApochromat objective on a Zeiss LSM880 confocal microscope used in Airyscan mode and processed using Zen Black software (Zeiss).

CTL-target conjugates were formed by mixing equal numbers of day 5 post-activation CTLs and P815-blue target cells in the presence of 1 μg/ml of anti-CD3ε for 20 min at 37°C, 10% CO_2. Cells were allowed to adhere on slides, fixed in ice-cold methanol for 5 min, blocked in PBS, 1% BSA and incubated with anti-γ-tubulin, anti-LAMP1 (supernatant, 1D4B), and Alexa Fluor 488-conjugated anti-CD8. After washing cells were labeled with Alexa Fluor 546-conjugated anti-mouse IgG and Alexa Fluor 647-conjugated anti-rabbit IgG. Conjugate

formation was imaged using an Andor Revolution spinning disk microscope with a Leica DMi8 microscope, Yokogawa CSU-X1 spinning disk, Andor Technology iXon Ultra 888 EMCCD camera and Fusion software. Samples were imaged using an Olympus Plan Apochromat 100 Å~ 1.4NA oil objective and *z*-step distances of 0.5 µm.

Nucleofection with Lifeact-mApple and mt-Keima

CTLs were nucleofected with 5 µg of plasmid DNA using P3 Primary cell nucleofector solution using the primary mouse T cell program of the 4D-Nucleofector system. Post-nucleofection, cells were incubated for at 37°C, 10% CO_2 in mouse T Cell nucleofector medium with 10% FBS, 2 mM L-glutamine, and 0.01% DMSO. Cells were split after 4 hours into mouse T cell media and allowed to recover for at least 18 hours at 37°C, 10% CO_2.

Live-cell microscopy and quantification of cell migration and mitophagy

CTLs (5 days post activation) were plated in dishes with a coverslip insert (pre-coated with 0.5 µg/ml of ICAM-1/CD45 Fc) in CO_2-independent media with 10% FBS and 2 mM L-glutamine, and imaged for 5 min at 37°C. All live microscopy samples were imaged on a Zeiss LSM 780 with Zen Black software, using a Zeiss 63X 1.4NA PlanApochromat objective. Cell migration was quantified in CTLs (5 days after activation) expressing Lifeact-mApple, with nuclei stained with Hoechst, excited at 561 nm and 405 nm, respectively. The speed of CTL migration was quantified using the TrackMate plugin of ImageJ v1.52 (NIH), to track the motion of nuclei as an indicator of cell migration. Mitophagy was detected in CTLs expressing mt-Keima, excited at 488 nm (optimal excitation at pH=8) and 561 nm (optimal excitation at pH=4.5). The Imaris spot tracking function was used to filter the mt-Keima signal and calculate the mean fluorescence intensity (MFI) for each object. Spots were defined as “red” (mitolysosomes) when red MFI >2X green MFI. The percentage mitophagy was calculated from the number of red spots divided by the sum of green and red spots.

Transmission electron microscopy

$CD8^+$ cells were purified using flow cytometry-based sorting 4 days post activation, using Zombie Aqua and APC-conjugated anti-CD8 and allowed to recover for up to 24 hours in CTL media at 37°C, 10% CO_2. CTL were washed and resuspended in serum-free RPMI, plated in four-well plastic tissue culture plates (Nunc) at 2×10^6 per sample and allowed to adhere at 37°C for 20 min. CTLs were fixed in 2% PFA/1.5% glutaraldehyde, washed and post-fixed in 1% osmium followed by 0.5% uranyl acetate, and processed for EPON embedding as described (*39*). Samples were from three independent biological replicates with two or more technical replicates analyzed per preparation. Sections (60-80 nm) were post-stained with lead citrate and viewed using a FEI Tecnai G2 Spirit BioTWIN transmission EM. Images were captured using a Gatan 4K US1000 CCD camera and FEI TIA software (v 4.7 SP3). For quantitation of mitochondria phenotype, images were collected of every cell profile within four (WT=128 cells total) or five (KO=154 cells total) grid squares of a single thin section (60-80 nm) of each of the WT and KO CTL samples. Each cell profile was scored for mitochondrial morphology as follows: none (no mitochondria), normal (normal mitochondria) and disrupted (mitochondria with disrupted cristae). For quantitation of lytic granule number and cross-sectional area, images were collected of every cell profile within four (WT=139 cells total) or five (KO=164 cells total) grid squares of a single thin section for WT and KO CTL samples. Cross sectional area (nm^2) was calculated using the lasso tool in Adobe Photoshop (CC 2019).

Seahorse Mito Stress Assay

Analysis of mitochondrial respiration and glycolytic rate of day 5 post-activation CTLs was performed using a Seahorse XFe96 extracellular flux analyzer with a Seahorse XF Cell Mito Stress Test Kit following manufacturer's instructions. The Seahorse XFe96 FluxPak cartridge was hydrated with distilled water overnight at 37°C (no CO_2) and equilibrated for 1 hour on the day of the assay in Seahorse XF Calibrant solution. Vessels were pre-coated with 22.4 µg/ml of Cell-Tak for 20 min at 37°C to ensure continued adhesion of CTLs on the plate during

the assay. DMEM used in the assay was supplemented with 10 mM glucose, 1 mM sodium pyruvate, and 2 mM L-glutamine, with pH adjusted to 7.4. To test the oxygen consumption rate (OCR) and extracellular acidification rate (ECAR), 1 μM oligomycin, 1 μM FCCP, and 0.5 μM rotenone/antimycin A were loaded at the indicated times. Seahorse data were collected using Wave Controller 2.6 (Agilent).

HPG protein synthesis assay

Protein synthesis was assayed using the Click-iT HPG-AF488 Protein Synthesis Assay Kit. CTLs (5 days after activation) were washed and incubated for 30 min at 37°C in methionine-free RPMI supplemented as for CTL culture medium. Protein synthesis was measured by addition of 100 μM Click-IT L-homoproparglycine (HPG) to the media. Cycloheximide (100 μg/ml) was added to control samples to inhibit cytosolic translation. Cells were plated ±2 μg/ml of anti-CD3ε at 37°C, 10% CO_2 for 1 hour to allow for HPG incorporation.

Cells were then labeled with Zombie Violet and Brilliant Violet 711-conjugated anti-CD8 for 20 min at 4°C. Samples were fixed in 3.7% PFA for 15 min at room temperature, washed in PBS, 3% BSA and permeabilized in PBS, 0.5% Triton X-100 and washed again in PBS, 3% BSA before HPG labeling through click-chemistry using azide-conjugated Alexa Fluor 488 and washed in rinse buffer as indicated in manufacturer's protocol. Cells were resuspended in PBS and analyzed on an Attune NxT.

Mitochondrial protein synthesis was assayed by washing and incubating CTLs (5 days after activation) in T cell media using methionine-free RPMI and FBS dialysed against PBS (to remove methionine). After 30 min at 37°C in methionine-free media, 100 μg/ml of cycloheximide was added to inhibit cytosolic translation and 100 μM Click-IT L-homoproparglycine (HPG) was added for 1-1.5 hours at 37°C, 10% CO_2 to label protein synthesis in the mitochondria. CTLs were then washed in serum-free RPMI and allowed to adhere to slides at 37°C, 10% CO_2 for 10-15 min before fixation with 3.7% PFA for 15 min at

37°C. Cells were permeabilized for 20 min in 0.5% Triton X-100 and HPG was labeled through click-chemistry using azide-conjugated AF488. Samples were then washed in PBS and mitochondria were labeled using anti-PDH (2 hours) and anti-mouse-AF546 for 1 hour, at room temperature. Nuclei were stained using 200 ng/ml Hoechst 33342, mounted in ProLong Diamond and imaged using the Andor Revolution spinning disk microscope as described above.

Intracellular cytokine staining

WT and *Usp30*$^{-/-}$ CTLs (5 days after initial activation) incubated ±2 μg/ml of plate-bound anti-CD3ε for 4.5 hours at 37°C, 10% CO_2 were treated with GolgiStop (monensin), washed in PBS at 4°C, stained with Zombie Violet and Brilliant Violet 711-conjugated anti-CD8a for 20 min at 4°C, washed in PBS, 10% FBS and fixed and permeabilized using the Foxp3 Transcription Factor Staining Buffer following the manufacturer's protocol and labeled with antibodies to IFNγ and TNFα for 30 min at room temperature. Cells were rinsed in permeabilization buffer and PBS, resuspended in PBS and analyzed using an Attune NxT.

ATP assay

ATP measurements were performed using the ATP Determination Kit. WT and *Usp30*$^{-/-}$ CTLs (5 days after activation) were incubated ±2 μg/ml of plate-bound anti-CD3ε for 4.5 hours at 37°C, 10% CO_2. Two million cells per sample were washed in PBS and lysed in distilled water by boiling at 90°C for 5 min as described before (*40*) before the supernatant was cleared by centrifugation at 18,800*g* for 10 min at 4°C. Control samples were treated with 25 μM oligomycin and 100 mM 2-deoxy-D-glucose (2-DG) to distinguish mitochondrial derived ATP from glycolysis-derived ATP, respectively, and lysed as above. ATP standards and ATP reaction buffer were prepared as indicated by manufacturer. The ATP concentration was quantified by measured by luminescence at 560 nm, using a SpectraMax M5 spectrophotometer and SoftMaxPro 5.4.1 (Molecular Devices).

Cytof sample processing and analysis

CTLs (5-7 days after activation) ±1 μg/ml of plate-bound CD3ε (145-2C11) for 1 hour at 37°C were stained using MaxPar reagent kits (Fluidigm) using metal-conjugated antibodies as described (*41*).

Mass spectrometry processing and analysis

CTLs (5 days after activation) were incubated ±2 μg/ml of plate-bound CD3ε (500A2) for 4.5 hours at 37°C. Cytosolic translation was inhibited with 100 μg/ml of cycloheximide and mitochondrial translation with 10 μg/ml of doxycyline (DOX) for 4-4.5 hours. Five million CTLs per sample were then washed twice in ice-cold PBS and flash-frozen on dry ice prior to processing for mass spectrometry.

Protein lysates were generated from cell pellets as per (*42*) but using a lysis buffer of 5% SDS, 50 mM TEAB pH 8.5, and 10 mM TCEP. Protein clean up and peptide generation was performed by the S-Trap method (*43*) as per manufacturer protocol (Protifi) and as previously described (*44*).

For WT/KO and CHX-treated samples, 2 μg of peptide was analyzed per sample. Samples were injected onto a nanoscale C18 reverse-phase chromatography system (UltiMate 3000 RSLC nano, ThermoFisher) then electrosprayed into an Q Exactive HF-X Mass Spectrometer (Thermo Scientific) as described in (*44*). Analysis for doxycycline-treated samples had the following differences: 1.5 μg peptide was injected per sample, analysis was performed on Orbitrap Exploris 480 Mass Spectrometer (ThermoFisher), sample were loaded at 10 μl/min onto trap column and the easy spray source operated in positive mode with spray voltage at 2.445 kV, and the ion transfer tube temperature at 250°C.

The data were processed, searched, and quantified with Spectronaut (*45*) 14 using the directDIA option using the same analysis settings as (*44*). The directDIA data were searched against a mouse hybrid database from databases in July 2019 Uniprot release described in (*42*).

Protein copy number quantification was performed in the Perseus software package, version 1.6.6.0. Mean copy number per cell was calculated using the "proteomic ruler" plugin as previously described (*46*). The mass spectrometry proteomics data have been deposited to the ProteomeXchange Consortium via the PRIDE (*47*) partner repository with the dataset identifiers PXD021508 (*Usp30*$^{-/-}$, CHX) and PXD026948 (DOX).

Flow cytometry and statistical analysis

All flow cytometry data was acquired using the BD FACSDIVA (BD Biosciences) or Attune NxT software (ThermoFisher) and analyzed using FlowJo v10. Microscopy images were rendered and analyzed using Imaris 9 software (Bitplane). Student's *t* test was used to determine statistical significance as indicated in the figure legends. Graphs were generated using Prism 8 (GraphPad Software).

For mass spectrometry data, copy number values were used to calculate fold change (FC). *P*-values were calculated using a two-tailed paired Student's *t* test and applying a false discovery rate (FDR) correction based on the Benjamini–Hochberg method. Analysis was performed in Microsoft Excel and RStudio. Copy number values were displayed as a heat map using Morpheus (Broad), whereas pie charts indicating cellular compartments were visualized using Prism 8 (GraphPad). Volcano plots were generated by plotting $\log_2$(FC) and $\log_{10}(P)$ for all peptides on Tableau Interactive Dashboard 2020 and highlighting FDR based on the Benjamini–Hochberg method.

Protein cellular localization was manually curated based on UniProt annotations (https://www.uniprot.org/). Mass contribution of proteins (grams per cell) was calculated as (protein copy number/cell) × (molecular weight (Daltons))/(Avogadro's constant). The percentage of mitochondrial protein content of mitochondrial ribosomes was calculated by defining total mitochondrial proteins as the proteins from in the Mouse MitoCarta 2.0 database (*48*) and mitochondrial ribosomal proteins on the protein description terms "ribosomal protein"

and “mitochondrial”. Cytosolic ribosomal proteins were defined by the KEGG term “ribosome”. Moonlighting metabolic enzymes were based on their RNA-binding protein (RBP) ability, as previously reported (*32*, *33*, *49-51*). For gene ontology (GO) enrichment analysis, values for FC and FDR correction were compared for proteins detected in the mass spectrometry of both KO vs WT and DOX-treated vs untreated CTLs (all unstimulated). Proteins with corrected *P*-values below the 10% FDR statistical threshold were selected for further analysis. GO enrichment (http://geneontology.org/) (*52*, *53*) was analyzed by detecting overrepresented “biological process” in the list of commonly downregulated proteins in KO and DOX-treated CTLs.

References and Notes:

1. P. Golstein, G. M. Griffiths, An early history of T cell-mediated cytotoxicity. *Nat Rev Immunol* **18**, 527-535 (2018).

2. C. J. Sanderson, The mechanism of T cell mediated cytotoxicity II. Morphological studies of cell death by time-lapse microcinematography, *Proc R Soc Lond* **192**, 241-255. (1976).

3. T. L. Rothstein, M. Mage, G. Jones, L. L. McHugh, Cytotoxic T lymphocyte sequential killing of immobilized allogeneic tumor target cells measured by time-lapse microcinematography. *J Immunol* **121**, 1652-1656 (1978).

4. A. Wiedemann, D. Depoil, M. Faroudi, S. Valitutti, Cytotoxic T lymphocytes kill multiple targets simultaneously via spatiotemporal uncoupling of lytic and stimulatory synapses. *Proc Natl Acad Sci U S A* **103**, 10985-10990 (2006).

5. M. Fischer, G. R. Bantug, S. Dimeloe, P. M. Gubser, A.-V. Burgener, J. Grählert, M. L. Balmer, L. Develioglu, R. Steiner, G. Unterstab, U. Sauder, G. Hoenger, C. Hess, Early effector maturation of naïve human $CD8^+$ T cells requires mitochondrial biogenesis. *European Journal of Immunology* **48**, 1632-1643 (2018).

6. M. D. Buck, D. O'Sullivan, R. I. Klein Geltink, J. D. Curtis, C. H. Chang, D. E. Sanin, J. Qiu, O. Kretz, D. Braas, G. J. van der Windt, Q. Chen, S. C. Huang, C. M. O'Neill, B. T. Edelson, E. J. Pearce, H. Sesaki, T. B. Huber, A. S. Rambold, E. L. Pearce, Mitochondrial Dynamics Controls T Cell Fate through Metabolic Programming. *Cell* **166**, 63-76 (2016).

7. G. J. van der Windt, D. O'Sullivan, B. Everts, S. C. Huang, M. D. Buck, J. D. Curtis, C. H. Chang, A. M. Smith, T. Ai, B. Faubert, R. G. Jones, E. J. Pearce, E. L. Pearce,

CD8 memory T cells have a bioenergetic advantage that underlies their rapid recall ability. *Proc Natl Acad Sci U S A* **110**, 14336-14341 (2013).

8. N. E. Scharping, A. V. Menk, R. S. Moreci, R. D. Whetstone, R. E. Dadey, S. C. Watkins, R. L. Ferris, G. M. Delgoffe, The Tumor Microenvironment Represses T Cell Mitochondrial Biogenesis to Drive Intratumoral T Cell Metabolic Insufficiency and Dysfunction. *Immunity* **45**, 701-703 (2016).

9. A. D. D'Souza, N. Parikh, S. M. Kaech, G. S. Shadel, Convergence of multiple signaling pathways is required to coordinately up-regulate mtDNA and mitochondrial biogenesis during T cell activation. *Mitochondrion* **7**, 374-385 (2007).

10. A. J. M. Howden, J. L. Hukelmann, A. Brenes, L. Spinelli, L. V. Sinclair, A. I. Lamond, D. A. Cantrell, Quantitative analysis of T cell proteomes and environmental sensors during T cell differentiation. *Nat Immunol* **20**, 1542-1554 (2019).

11. E. L. Pearce, M. C. Poffenberger, C. H. Chang, R. G. Jones, Fueling immunity: insights into metabolism and lymphocyte function. *Science* **342**, 1242454 (2013).

12. A. V. Menk, N. E. Scharping, R. S. Moreci, X. Zeng, C. Guy, S. Salvatore, H. Bae, J. Xie, H. A. Young, S. G. Wendell, G. M. Delgoffe, Early TCR Signaling Induces Rapid Aerobic Glycolysis Enabling Distinct Acute T Cell Effector Functions. *Cell Rep* **22**, 1509-1521 (2018).

13. M. Giacomello, A. Pyakurel, C. Glytsou, L. Scorrano, The cell biology of mitochondrial membrane dynamics. *Nat Rev Mol Cell Biol* **21**, 204-224 (2020).

14. L. Montava-Garriga, I. G. Ganley, Outstanding Questions in Mitophagy: What We Do and Do Not Know. *J Mol Biol* **432**, 206-230 (2020).

15. N. Nakamura, S. Hirose, Regulation of mitochondrial morphology by USP30, a deubiquitinating enzyme present in the mitochondrial outer membrane. *Mol Biol Cell* **19**, 1903-1911 (2008).

16. B. Bingol, J. S. Tea, L. Phu, M. Reichelt, C. E. Bakalarski, Q. Song, O. Foreman, D. S. Kirkpatrick, M. Sheng, The mitochondrial deubiquitinase USP30 opposes parkin-mediated mitophagy. *Nature* **510**, 370-375 (2014).

17. E. Marcassa, A. Kallinos, J. Jardine, E. V. Rusilowicz-Jones, A. Martinez, S. Kuehl, M. Islinger, M. J. Clague, S. Urbé, Dual role of USP30 in controlling basal pexophagy and mitophagy. *EMBO Rep* **19**, e45595-e45595 (2018).

18. L. Abeler-Dörner, A. G. Laing, A. Lorenc, D. S. Ushakov, S. Clare, A. O. Speak, M. A. Duque-Correa, J. K. White, R. Ramirez-Solis, N. Saran, K. R. Bull, B. Morón, J. Iwasaki, P. R. Barton, S. Caetano, K. I. Hng, E. Cambridge, S. Forman, T. L. Crockford, M. Griffiths, L. Kane, K. Harcourt, C. Brandt, G. Notley, K. O. Babalola, J. Warren, J. C. Mason, A. Meeniga, N. A. Karp, D. Melvin, E. Cawthorne, B. Weinrick, A. Rahim, S. Drissler, J. Meskas, A. Yue, M. Lux, G. X. Song-Zhao, A. Chan, C. Ballesteros Reviriego, J. Abeler, H. Wilson, A. Przemska-Kosicka, M. Edmans, N. Strevens, M. Pasztorek, T. F. Meehan, F. Powrie, R. Brinkman, G. Dougan, W. Jacobs, C. M. Lloyd, R. J. Cornall, K. J. Maloy, R. K. Grencis, G. M. Griffiths, D. J. Adams, A. C. Hayday,

High-throughput phenotyping reveals expansive genetic and structural underpinnings of immune variation. *Nat Immunol* **21**, 86-100 (2020).

19. L. Phu, C. M. Rose, J. S. Tea, C. E. Wall, E. Verschueren, T. K. Cheung, D. S. Kirkpatrick, B. Bingol, Dynamic Regulation of Mitochondrial Import by the Ubiquitin System. *Mol Cell* **77**, 1107-1123 e1110 (2020).

20. N. Sun, J. Yun, J. Liu, D. Malide, C. Liu, I. I. Rovira, K. M. Holmström, M. M. Fergusson, Y. H. Yoo, C. A. Combs, T. Finkel, Measuring In Vivo Mitophagy. *Mol Cell* **60**, 685-696 (2015).

21. C. A. Ingraham, L. S. Burwell, J. Skalska, P. S. Brookes, R. L. Howell, S. S. Sheu, C. A. Pinkert, NDUFS4: creation of a mouse model mimicking a Complex I disorder. *Mitochondrion* **9**, 204-210 (2009).

22. S. Campello, R. A. Lacalle, M. Bettella, S. Mañes, L. Scorrano, A. Viola, Orchestration of lymphocyte chemotaxis by mitochondrial dynamics. *The Journal of Experimental Medicine* **203**, 2879-2886 (2006).

23. R. Uellner, M. J. Zvelebil, J. Hopkins, J. Jones, L. K. MacDougall, B. P. Morgan, E. Podack, M. D. Waterfield, G. M. Griffiths, Perforin is activated by a proteolytic cleavage during biosynthesis which reveals a phospholipid-binding C2 domain. *The EMBO journal* **16**, 7287-7296 (1997).

24. K. Araki, M. Morita, A. G. Bederman, B. T. Konieczny, H. T. Kissick, N. Sonenberg, R. Ahmed, Translation is actively regulated during the differentiation of $CD8^+$ effector T cells. *Nat Immunol* **18**, 1046-1057 (2017).

25. S. Isaaz, K. Baetz, K. Olsen, E. Podack, G. M. Griffiths, Serial killing by cytotoxic T lymphocytes: T cell receptor triggers degranulation, re-filling of the lytic granules and secretion of lytic proteins via a non-granule pathway. *European Journal of Immunology* **25**, 1071-1079 (1995).

26. E. L. Pearce, A. C. Mullen, G. A. Martins, C. M. Krawczyk, A. S. Hutchins, V. P. Zediak, M. Banica, C. B. DiCioccio, D. A. Gross, C. A. Mao, H. Shen, N. Cereb, S. Y. Yang, T. Lindsten, J. Rossant, C. A. Hunter, S. L. Reiner, Control of effector $CD8^+$ T cell function by the transcription factor Eomesodermin. *Science* **302**, 1041-1043 (2003).

27. U. Topf, B. Uszczynska-Ratajczak, A. Chacinska, Mitochondrial stress-dependent regulation of cellular protein synthesis. *J Cell Sci* **132**, jcs226258 (2019).

28. F. Boos, J. Labbadia, J. M. Herrmann, How the Mitoprotein-Induced Stress Response Safeguards the Cytosol: A Unified View. *Trends Cell Biol* **30**, 241-254 (2020).

29. D. O'Sullivan, M. A. Stanczak, M. Villa, F. M. Uhl, M. Corrado, R. I. Klein Geltink, D. E. Sanin, P. Apostolova, N. Rana, J. Edwards-Hicks, K. M. Grzes, A. M. Kabat, R. L. Kyle, M. Fabri, J. D. Curtis, M. D. Buck, A. E. Patterson, A. Regina, C. S. Field, F. Baixauli, D. J. Puleston, E. J. Pearce, R. Zeiser, E. L. Pearce, Fever supports $CD8^+$ effector T cell responses by promoting mitochondrial translation. *Proc Natl Acad Sci U S A* **118**, e2023752118 (2021).

30. L. Almeida, A. Dhillon-LaBrooy, C. N. Castro, N. Adossa, G. M. Carriche, M. Guderian, S. Lippens, S. Dennerlein, C. Hesse, B. N. Lambrecht, L. Berod, L. Schauser, B. R. Blazar, M. Kalesse, R. Muller, L. F. Moita, T. Sparwasser, Ribosome-Targeting Antibiotics Impair T Cell Effector Function and Ameliorate Autoimmunity by Blocking Mitochondrial Protein Synthesis. *Immunity* **54**, 68-83 e66 (2021).

31. M. Zorkau, C. A. Albus, R. Berlinguer-Palmini, Z. M. A. Chrzanowska-Lightowlers, R. N. Lightowlers, High-resolution imaging reveals compartmentalization of mitochondrial protein synthesis in cultured human cells. *Proc Natl Acad Sci U S A* **118**, e2008778118 (2021).

32. A. Castello, M. W. Hentze, T. Preiss, Metabolic Enzymes Enjoying New Partnerships as RNA-Binding Proteins. *Trends Endocrinol Metab* **26**, 746-757 (2015).

33. M. Turner, M. D. Diaz-Munoz, RNA-binding proteins control gene expression and cell fate in the immune system. *Nat Immunol* **19**, 120-129 (2018).

34. F. Salerno, M. Turner, M. C. Wolkers, Dynamic Post-Transcriptional Events Governing $CD8^+$ T Cell Homeostasis and Effector Function. *Trends Immunol* **41**, 240-254 (2020).

35. C. H. Chang, J. D. Curtis, L. B. Maggi, B. Faubert, A. V. Villarino, D. O'Sullivan, S. C. C. Huang, G. J. W. Van Der Windt, J. Blagih, J. Qiu, J. D. Weber, E. J. Pearce, R. G. Jones, E. L. Pearce, Posttranscriptional control of T cell effector function by aerobic glycolysis. *Cell* **153**, 1239-1239 (2013).

36. F. Buttgereit, M. D. Brand, A hierarchy of ATP-consuming processes in mammalian cells. *Biochem J* **312**, 163-167 (1995).

37. A. T. Ritter, Y. Asano, J. C. Stinchcombe, N. M. Dieckmann, B. C. Chen, C. Gawden-Bone, S. van Engelenburg, W. Legant, L. Gao, M. W. Davidson, E. Betzig, J. Lippincott-Schwartz, G. M. Griffiths, Actin depletion initiates events leading to granule secretion at the immunological synapse. *Immunity* **42**, 864-876 (2015).

38. L. O. Randzavola, K. Strege, M. Juzans, Y. Asano, J. C. Stinchcombe, C. M. Gawden-Bone, M. N. Seaman, T. W. Kuijpers, G. M. Griffiths, Loss of ARPC1B impairs cytotoxic T lymphocyte maintenance and cytolytic activity. *J Clin Invest* **129**, 5600-5614 (2019).

39. M. R. Jenkins, A. Tsun, J. C. Stinchcombe, G. M. Griffiths, The strength of T cell receptor signal controls the polarization of cytotoxic machinery to the immunological synapse. *Immunity* **31**, 621-631 (2009).

40. H. S. Garewal, F. R. Ahmann, R. B. Schifman, A. Celniker, ATP assay: ability to distinguish cytostatic from cytocidal anticancer drug effects. *J Natl Cancer Inst* **77**, 1039-1045 (1986).

41. C. Y. Ma, J. C. Marioni, G. M. Griffiths, A. C. Richard, Stimulation strength controls the rate of initiation but not the molecular organisation of TCR-induced signalling. *Elife* **9**, e53948 (2020).

42. J. M. Marchingo, L. V. Sinclair, A. J. Howden, D. A. Cantrell, Quantitative analysis of how Myc controls T cell proteomes and metabolic pathways during T cell activation. *Elife* **9**, (2020).

43. A. Zougman, P. J. Selby, R. E. Banks, Suspension trapping (STrap) sample preparation method for bottom-up proteomics analysis. *Proteomics* **14**, 1006-1000 (2014).

44. L. Reyes, A. S.-G. M, T. Morrison, A. J. M. Howden, E. R. Watts, S. Arienti, P. Sadiku, P. Coelho, A. S. Mirchandani, A. Zhang, D. Hope, S. K. Clark, J. Singleton, S. Johnston, R. Grecian, A. Poon, S. McNamara, I. Harper, M. H. Fourman, A. J. Brenes, S. Pathak, A. Lloyd, G. R. Blanco, A. von Kriegsheim, B. Ghesquiere, W. Vermaelen, C. T. Cologna, K. Dhaliwal, N. Hirani, D. H. Dockrell, M. K. B. Whyte, D. Griffith, D. A. Cantrell, S. R. Walmsley, -------A type I IFN, prothrombotic hyperinflammatory neutrophil signature is distinct for COVID-19 ARDS. *Wellcome Open Res* **6**, 38 (2021).

45. R. Bruderer, O. M. Bernhardt, T. Gandhi, S. M. Miladinovic, L. Y. Cheng, S. Messner, T. Ehrenberger, V. Zanotelli, Y. Butscheid, C. Escher, O. Vitek, O. Rinner, L. Reiter, Extending the limits of quantitative proteome profiling with data-independent acquisition and application to acetaminophen-treated three-dimensional liver microtissues. *Mol Cell Proteomics* **14**, 1400-1410 (2015).

46. J. R. Wisniewski, M. Y. Hein, J. Cox, M. Mann, A "proteomic ruler" for protein copy number and concentration estimation without spike-in standards. *Mol Cell Proteomics* **13**, 3497-3506 (2014).

47. Y. Perez-Riverol, A. Csordas, J. Bai, M. Bernal-Llinares, S. Hewapathirana, D. J. Kundu, A. Inuganti, J. Griss, G. Mayer, M. Eisenacher, E. Perez, J. Uszkoreit, J. Pfeuffer, T. Sachsenberg, S. Yilmaz, S. Tiwary, J. Cox, E. Audain, M. Walzer, A. F. Jarnuczak, T. Ternent, A. Brazma, J. A. Vizcaino, The PRIDE database and related tools and resources in 2019: improving support for quantification data. *Nucleic Acids Res* **47**, D442-D450 (2019).

48. S. E. Calvo, K. R. Clauser, V. K. Mootha, MitoCarta2.0: an updated inventory of mammalian mitochondrial proteins. *Nucleic Acids Res* **44**, D1251-1257 (2016).

49. B. M. Beckmann, R. Horos, B. Fischer, A. Castello, K. Eichelbaum, A. M. Alleaume, T. Schwarzl, T. Curk, S. Foehr, W. Huber, J. Krijgsveld, M. W. Hentze, The RNA-binding proteomes from yeast to man harbour conserved enigmRBPs. *Nat Commun* **6**, 10127 (2015).

50. E. D. Garcin, GAPDH as a model non-canonical AU-rich RNA binding protein. *Semin Cell Dev Biol* **86**, 162-173 (2019).

51. J. Ciesla, Metabolic enzymes that bind RNA: yet another level of cellular regulatory network? *Acta Biochim Pol* **53**, 11-32 (2006).

52. M. Ashburner, C. A. Ball, J. A. Blake, D. Botstein, H. Butler, J. M. Cherry, A. P. Davis, K. Dolinski, S. S. Dwight, J. T. Eppig, M. A. Harris, D. P. Hill, L. Issel-Tarver, A. Kasarskis, S. Lewis, J. C. Matese, J. E. Richardson, M. Ringwald, G. M. Rubin, G. Sherlock, Gene ontology: tool for the unification of biology. The Gene Ontology Consortium. *Nat Genet* **25**, 25-29 (2000).

53. C. Gene Ontology, The Gene Ontology resource: enriching a GOld mine. *Nucleic Acids Res* **49**, D325-D334 (2021).

Acknowledgements: We would like to thank R. Hegde, D. Ron, A. Brenes, M. Clague, M. Minczuk, A. Richard, and S. Urbé for their advice and helpful discussions, and C. Viscomi and M. Zeviani for spleens from *Ndufs4*$^{-/-}$ mice. We thank the Microscopy and Flow Cytometry facilities at the Cambridge Institute for Medical Research and the Fingerprints Proteomics Facility at the University of Dundee for technical assistance. **Funding:** This research was funded in whole, or in part, by the Wellcome Trust [Grant numbers 217100, 103930, 108415, 220543, 100156, 205023]. For the purpose of open access, the author has applied a CC BY public copyright licence to any Author Accepted Manuscript version arising from this submission. M.L. is supported by a PhD studentship from the Cambridge Institute for Medical Research, J.P by the Medical Research Council (Core grant MC_UU_0015/7) and J.M.M. by an Australian National Health and Medical Research Council CJ Martin early Career Fellowship. **Author contributions:** M.L. carried out all experimental work with the following exceptions: P.R.B. identified USP30 as a regulator of cytotoxicity and L.O.R initiated characterization; C.Y.M. provided CyTOF analysis and J.M.M. and D.A.C. support with analysis of mass spectrometry data. V.P. provided training for Seahorse assays and J.P. helpful discussions throughout. J.C.S. carried out electron microscopy and contributed throughout. M.L. and G.M.G. conceived the study, designed the experiments, and wrote the manuscript. **Competing interests:** Authors declare no competing interests; **Data and materials availability:** Mass spectrometry data are available via ProteomeXchange with identifier PXD021508 (*Usp30*$^{-/-}$) and PXD026948 (DOX). All other data are available in the main text or supplementary material.

Supplementary Materials:

Figures S1-S8

Tables S1-S5

Movies S1-S4

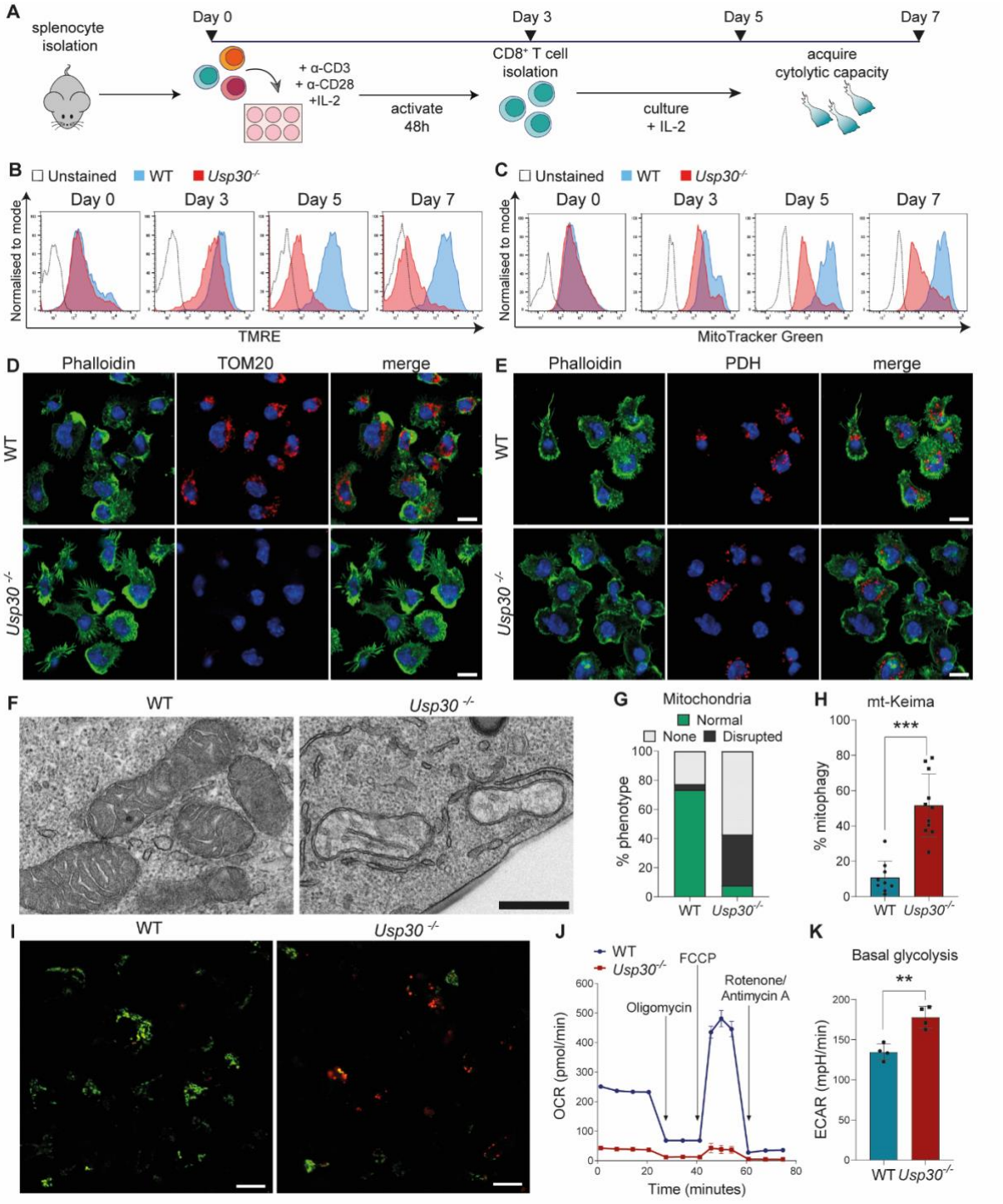

Fig. 1. *Usp30* deletion leads to mitochondrial depletion in effector CD8$^+$ T cells.

(A) Isolation and stimulation of murine primary CD8$^+$ T cells. (B and C) Time course of mitochondria labeled with (B) TMRE and (C) MitoTracker Green in WT and *Usp30*$^{-/-}$ naïve

$CD8^+$ T cells (day 0) as they mature into CTLs after stimulation (day 3-7). Immunofluorescence staining of (D) TOM20 (outer mitochondrial membrane) and (E) PDH (mitochondrial matrix) in day 5 WT and *Usp30*$^{-/-}$ (KO) CTLs. Scale bars=10 μm. (F) Transmission electron microscopy (TEM) sections (70 nm) of mitochondria in day 5 WT and *Usp30*$^{-/-}$ (KO) CTLs, scale bars=500 nm, and (G) quantitation of TEM images from 128 WT and 154 KO cell profiles. (H) Quantitation of live cell imaging of day 5 WT and *Usp30*$^{-/-}$ (KO) CTLs expressing mt-Keima. Each data point shows percentage of mitolysosomes (red mt-Keima signal) in a 63X field, indicative of mitophagy (>40 cells per genotype in each independent repeat). (I) Representative images of mt-Keima signal in day 5 WT and *Usp30*$^{-/-}$ (KO) CTLs. Scale bars=15 μm. (J) Mitochondrial respiratory capacity indicated by oxygen consumption rate (OCR) in day 5 WT and *Usp30*$^{-/-}$ (KO) CTLs. (K) Basal glycolysis in day 5 WT and *Usp30*$^{-/-}$ (KO) CTLs measured by extracellular acidification rate (ECAR) values at resting state. **=P<0.01, ***=P<0.001 (two-tailed unpaired Student's t test). Error bars show mean values ±SD of technical replicates in one representative experiment. All data are representative of at least three independent biological replicates.

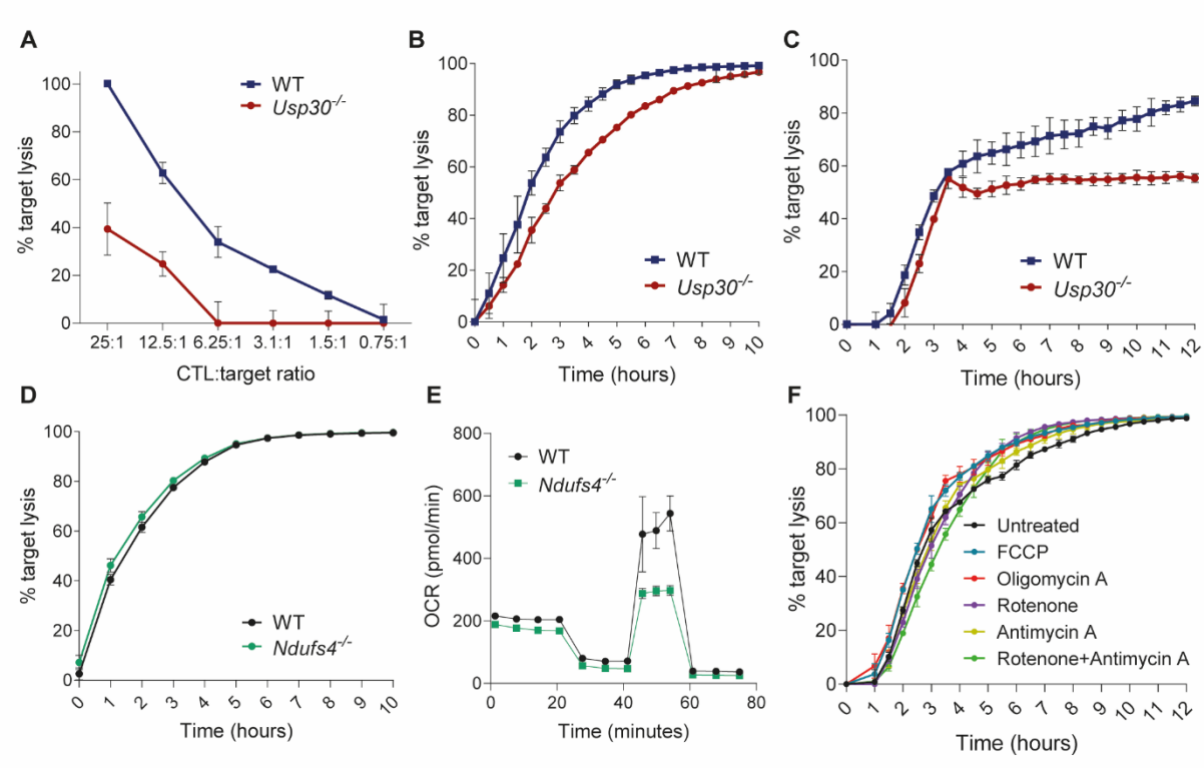

Fig. 2. Mitochondrial depletion leads to OXPHOS-independent inhibition of killing.

(A) Short-term (2.5 hours) killing assay with day 5 WT and *Usp30*$^{-/-}$ (KO) CTLs, varying CTL-to-target ratio. (B) Long-term (10 hours) killing assay showing percentage of target cell lysis over time (CTL-to-target ratio, 10:1) with day 5 WT and *Usp30*$^{-/-}$ (KO) CTLs. (C) Long-term (12 hours) killing assay showing percentage of target cell lysis over time (CTL-to-target ratio, 1:1) with day 5 WT and *Usp30*$^{-/-}$ (KO) CTLs. (D) Long-term (10 hours) killing assay showing percentage of target cell lysis over time (CTL-to-target ratio, 10:1) with day 5 WT and *Ndusf4*$^{-/-}$ CTLs. (E) Mitochondrial respiratory capacity shown by oxygen consumption rate (OCR) in day 5 WT and *Ndufs4*$^{-/-}$ CTLs. (F) Long-term (12 hours) killing assay showing percentage of target cell lysis over time (CTL-to-target ratio, 1:1) with day 5 WT CTL treated with inhibitors used in the Seahorse assay: Complex I (rotenone), III (antimycin A), V (oligomycin), and the uncoupling reagent, FCCP. Errors bars in show mean values ±SD of (A

to C and F) technical replicates, (D and E) biological replicates. All data are representative of at least two independent biological replicates.

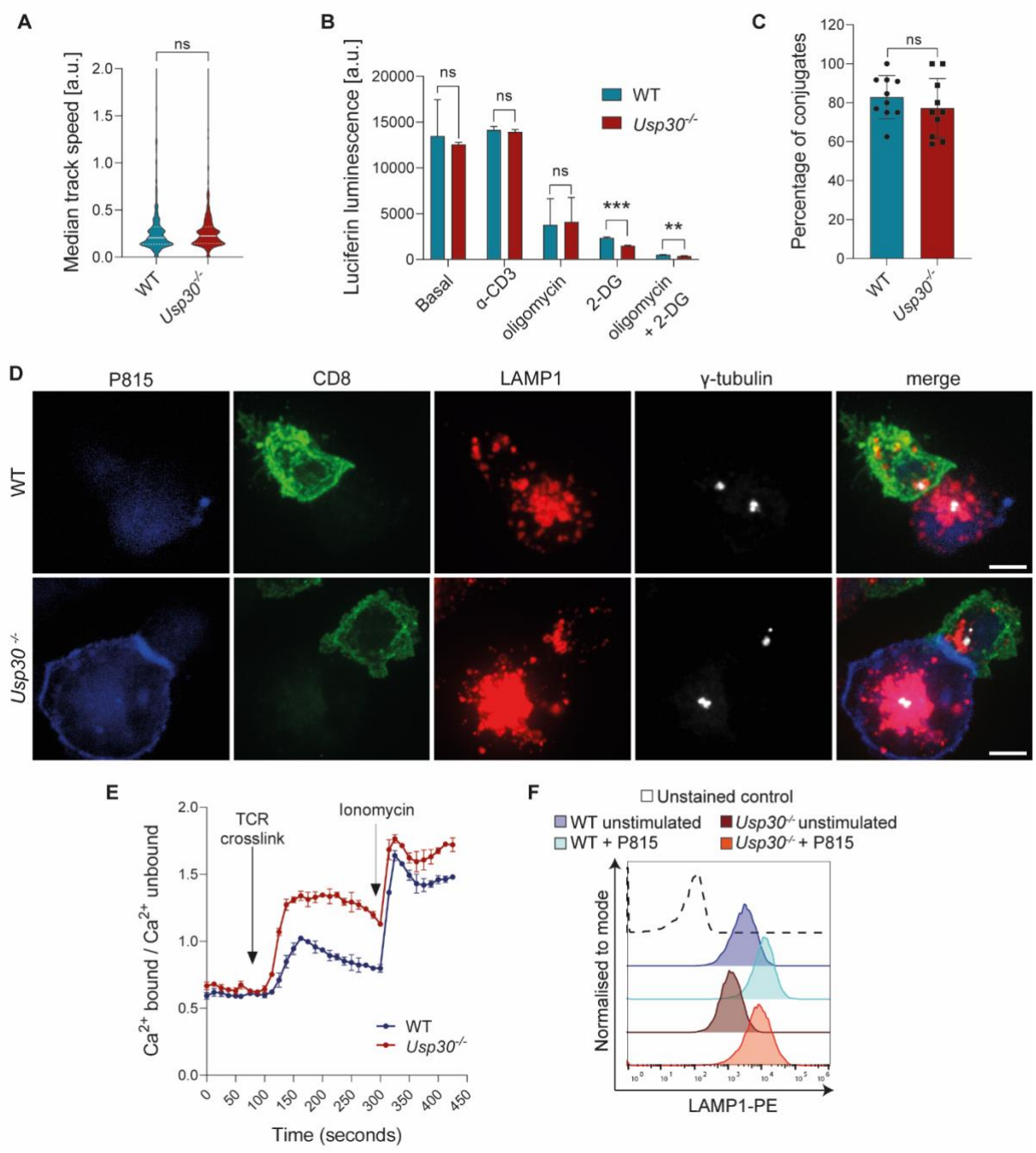

Fig. 3. Loss of USP30 does not impair ATP production, migration, target recognition or secretion.

(A) Track speed analysis of migrating day 5 WT and *Usp30*$^{-/-}$ (KO) CTLs (>200 cells per genotype per repeat; solid lines, median; dotted lines, quartiles). (B) ATP quantitation in day 5 WT and *Usp30*$^{-/-}$ (KO) CTLs, with (anti-CD3) or without (basal) TCR activation or treated

with oligomycin and/or 2-deoxy-D-glucose (2-DG) to account for mitochondria-derived and glycolysis-derived ATP respectively. (C) Quantitation of conjugate formation between day 5 WT and *Usp30*$^{-/-}$ (KO) CTLs and P815 target cells (>70 cells per genotype per independent repeat). Each dot shows the average percentage of conjugates in a 63X field. (D) Conjugates formed by day 5 WT or *Usp30*$^{-/-}$ (KO) CTLs (green) with P815 targets (blue) showing polarization of cytolytic granules (red) and centrosome (white). Scale bars=5 μm. (E) INDO-1 calcium assay showing changes in intracellular calcium concentration in day 5 WT and *Usp30*$^{-/-}$ (KO) CTLs before (t=0-60 s) and after TCR crosslinking (t=60 s) or ionomycin addition (t=300 s). (F) Histograms representing surface LAMP1-PE fluorescence intensity in day 5 WT and *Usp30*$^{-/-}$ (KO) CTLs before and after incubation with P815 target cells. a.u.=arbitrary unit. ns=not significant, **=P<0.01, ***=P<0.001 (unpaired two-tailed Student's *t* test). All error bars show mean values ±SD of technical replicates. Data are representative of three independent biological replicates.

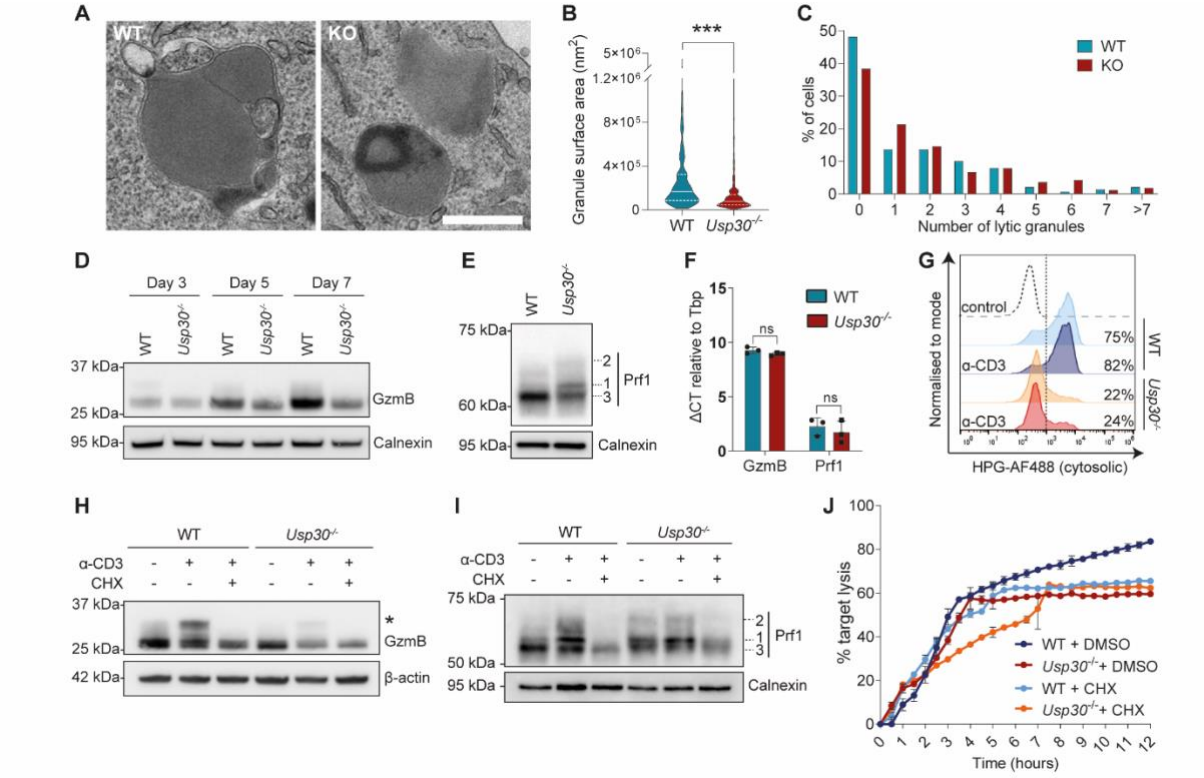

Fig. 4. Mitochondrial depletion leads to translation attenuation and reduced expression of key cytolytic proteins.

(A) TEM sections (70 nm) of lytic granules in day 5 WT and *Usp30*$^{-/-}$ (KO) CTLs, scale bar=500 nm, and quantitation of (B) cross-sectional surface areas, and (C) lytic granule number (solid line, median; dotted lines, quartiles) from 139 (WT) and 164 (KO) profiles. ***=P<0.001 (two-tailed unpaired Student's t test). Immunoblots showing (D) granzyme B (GzmB) and (E) perforin (Prf1) in WT and KO CTLs. Immature (1), intermediate (2), and mature (3) forms of perforin are labeled. (F) Granzyme B (GzmB) and perforin (Prf1) mRNA in day 5 WT and KO CTLs; ΔCT normalized to TATA-binding protein mRNA (Tbp). Error bars show mean values ±SD of three biological replicates. ns=not significant (two-tailed paired Student's t test). (G) HPG-AF488 incorporation (1 hour) into day 5 WT and *Usp30*$^{-/-}$ (KO) CTLs, ± anti-CD3 (TCR activation) where shown, or cycloheximide (CHX)-treated CTLs in

which cytosolic translation is inhibited (control). Immunoblots showing (H) granzyme B (GzmB) and (I) perforin (Prf1) in day 5 WT and *Usp30*$^{-/-}$ (KO) CTLs ±anti-CD3 or CHX. Newly synthesized GzmB indicated by (*). (J) Long-term (12 hours) killing assay with day 5 WT and *Usp30*$^{-/-}$ (KO) CTLs (CTL-to-target, 1:1), ±CHX. Error bars show mean values ±SD of technical replicates in one representative experiment. All data are representative of at least three independent biological replicates.

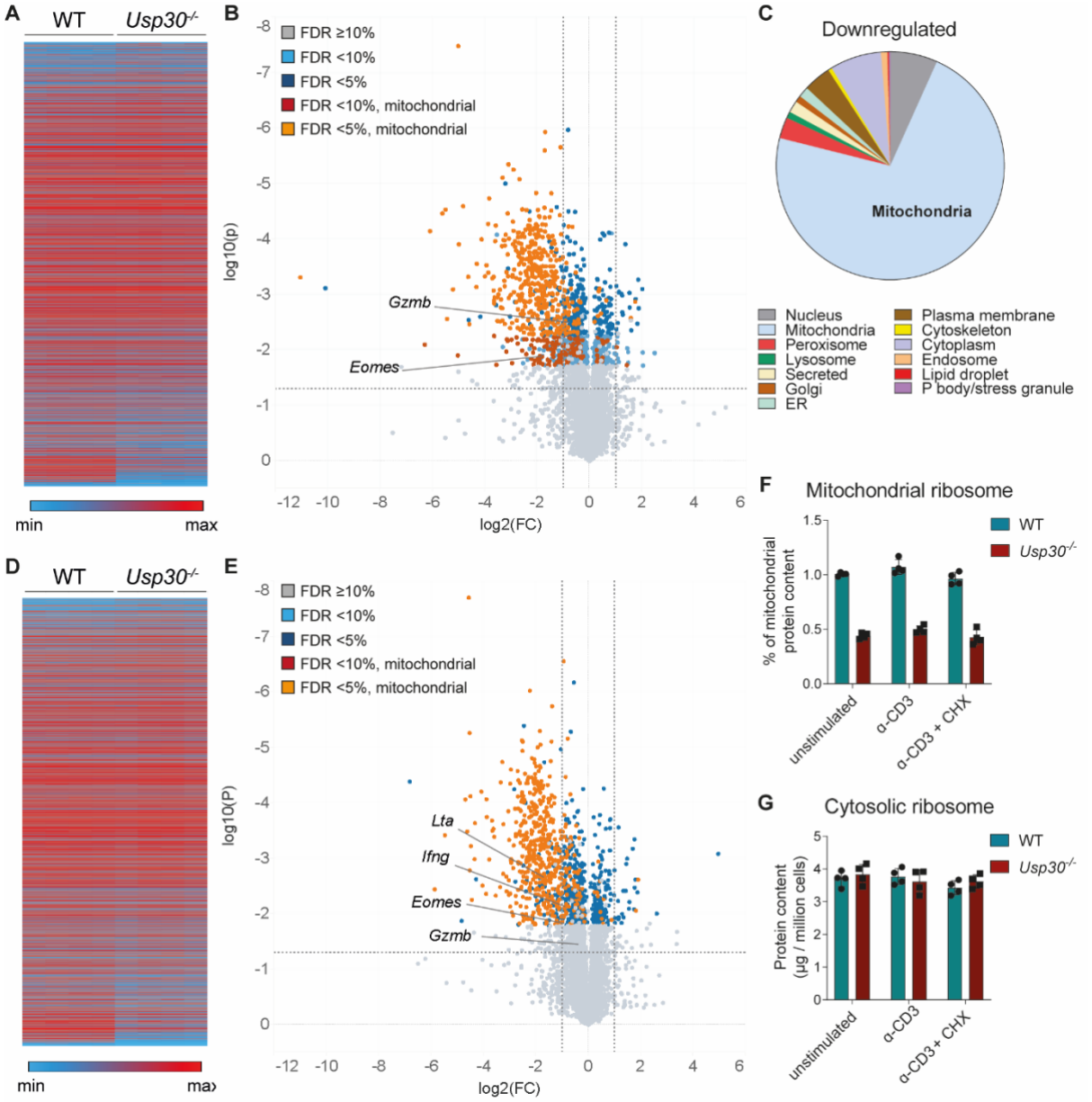

Fig. 5. Proteomic analysis of mitochondrially depleted *Usp30*$^{-/-}$ CTLs.

(A) Heat map showing global protein expression (protein copy number) in day 5 WT and *Usp30*$^{-/-}$ (KO) CTLs. (B) Volcano plot of upregulated (right quadrant) and downregulated (left quadrant) proteins in day 5 *Usp30*$^{-/-}$ (KO) CTLs compared to WT. Vertical bars denote $\log_2$(FC)=1,-1 and horizontal bar corresponds to the uncorrected *P*=0.05 threshold. Colored dots show hits within the 5% and 10% false discovery rate (FDR) range. GOCC-defined mitochondrial proteins are highlighted according to FDR. (C) Cellular localization of

downregulated proteins in day 5 *Usp30*$^{-/-}$ (KO) CTLs (5% FDR). (D) Heat map displaying global protein expression (protein copy number) in anti-CD3-stimulated (TCR activated, 4.5 hours) day 5 WT and *Usp30*$^{-/-}$ (KO) CTLs. (E) Volcano plot of upregulated and downregulated proteins in anti-CD3-stimulated day 5 *Usp30*$^{-/-}$ (KO) CTLs compared to WT. Quadrants and color scheme as in (B). Highlighted proteins are referenced by gene names in (B) and (E). (F) Percentage of mitochondrial ribosomal protein out of total mitochondrial peptides detected in unstimulated, anti-CD3 and CHX-treated day 5 CTLs. (G) Cytosolic ribosome protein expression in unstimulated, anti-CD3 and CHX-treated day 5 CTLs. Error bars show mean values ±SD from biological replicates (F and G). All data are representative of four biological replicates.

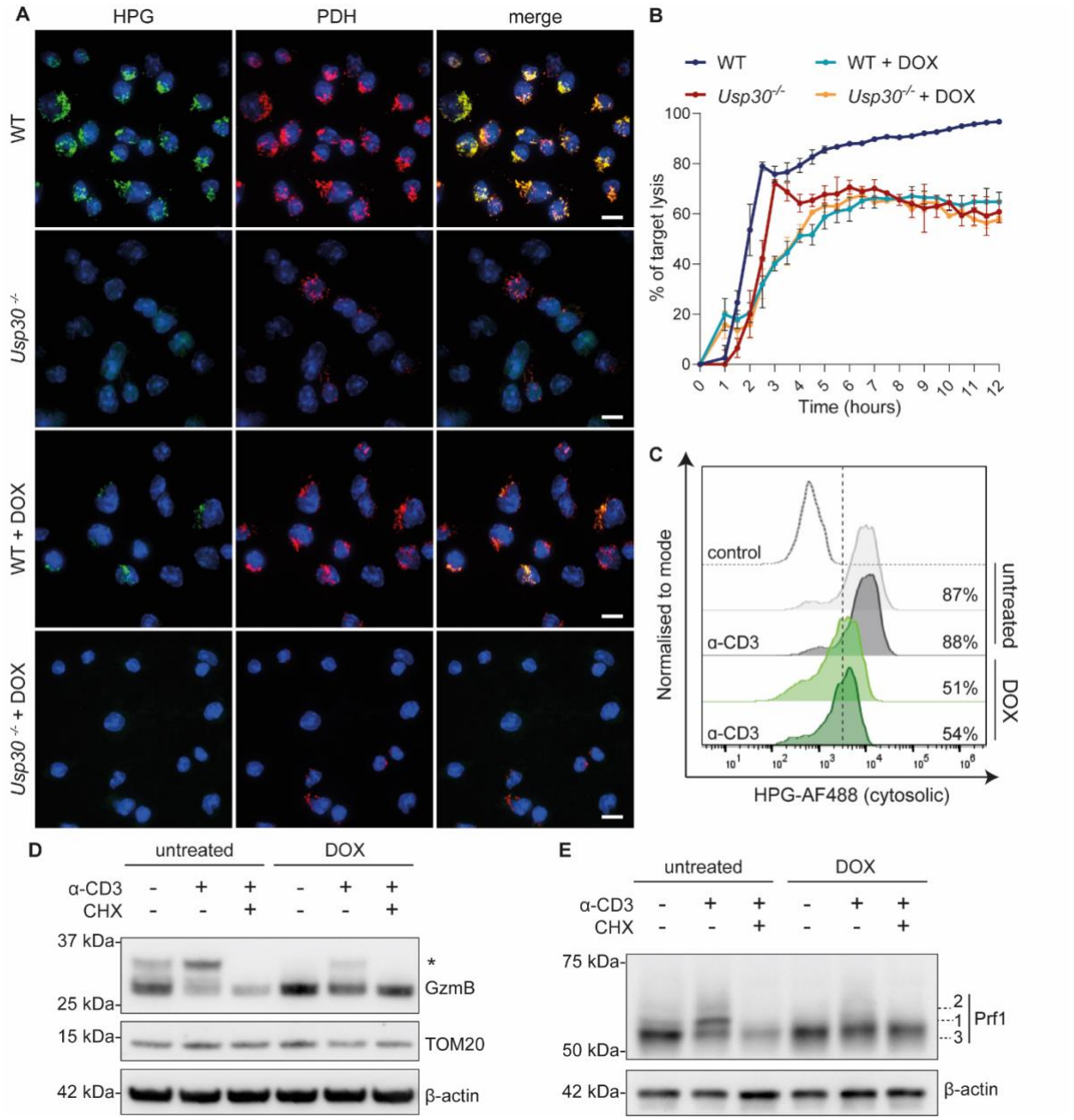

Fig. 6. Mitochondrial translation is required for sustained T cell killing.

(A) Immunofluorescence imaging of mitochondrial translation using 1-hour HPG-AF488 incorporation into day 5 WT and *Usp30*$^{-/-}$ (KO) CTLs treated with cycloheximide (CHX) to inhibit cytosolic translation. CTLs were either left untreated or treated with 10 μg/ml of doxycycline (DOX) to selectively inhibit mitochondrial translation as indicated. Scale bars=7 μm. (B) Long-term (12 hours) killing assay (CTL-to-target ratio, 1:1) showing percentage target lysis with day 5 WT and KO CTLs treated with DOX. Error bars show mean values ±SD

of technical replicates. (C) HPG-AF488 incorporation into day 5 WT CTLs treated for 1 hour with DOX to inhibit mitochondrial translation or CHX to inhibit cytosolic translation (control), stimulated with anti-CD3 (TCR) where shown. Immunoblots showing (D) Granzyme B (GzmB) and (E) perforin (Prf1) in day 5 WT CTLs treated with DOX and/or stimulated via TCR activation (anti-CD3) as indicated for 4 hours. Newly synthesized granzyme B indicated by (*). Immature (1), intermediate (2), and mature (3) forms of perforin are indicated. Error bars show mean values ±SD of technical replicates in one representative experiment. All data are representative of at least three independent biological replicates.

Supplementary Materials for

Mitochondrial translation is required for sustained killing by cytotoxic T cells

Miriam Lisci, Philippa R. Barton, Lyra O. Randzavola, Claire Y. Ma, Julia M. Marchingo, Doreen A. Cantrell, Vincent Paupe, Julien Prudent, Jane C. Stinchcombe, Gillian M. Griffiths

Correspondence to: gg305@cam.ac.uk

This PDF file includes:

Other Supplementary Materials for this manuscript include the following:

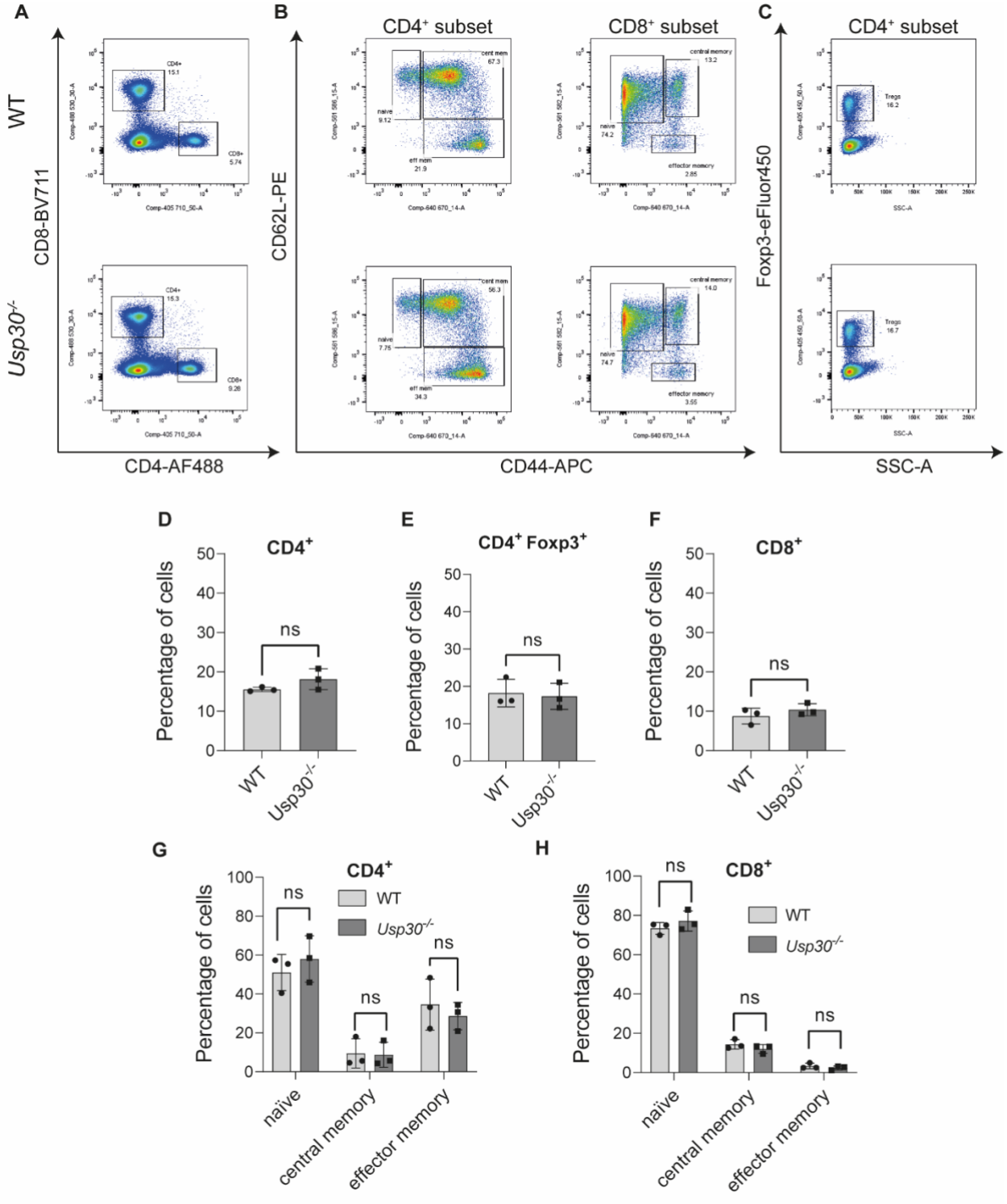
A
B
C
WT
Usp30-/-
CD8-BV711
CD4-AF488
CD62L-PE
CD44-APC
Foxp3-eFluor450
SSC-A
CD4+ subset
CD8+ subset
CD4+ subset
D
E
F
CD4+
CD4+ Foxp3+
CD8+
Percentage of cells
ns
WT
Usp30-/-
G
H
CD4+
CD8+
WT
Usp30-/-
naïve
central memory
effector memory

Fig. S1. Analysis of WT and *Usp30*$^{-/-}$ splenocytes.

(A) $CD4^+/CD8^+$ ratio in WT and *Usp30*$^{-/-}$ (KO) splenocytes. (B) $CD4^+$ and $CD8^+$ naïve ($CD62L^{hi}$, $CD44^{lo}$), central memory ($CD62L^{hi}$, $CD44^{hi}$) and effector memory ($CD62L^{lo}$, $CD44^{hi}$) T cell subsets in WT and *Usp30*$^{-/-}$ (KO) splenocytes. (C) Regulatory T cells ($CD4^+$, $Foxp3^+$) in WT and *Usp30*$^{-/-}$ (KO) splenocytes. (D to H) Quantitation of (D) $CD4^+$, (E) regulatory T cells, (F) $CD8^+$, (G) total $CD4^+$ and (H) $CD8^+$ subsets (naïve, central memory, and effector memory). Plots show the average of three biological replicates ±SD. ns=not significant (two-tailed paired Student's *t* test).

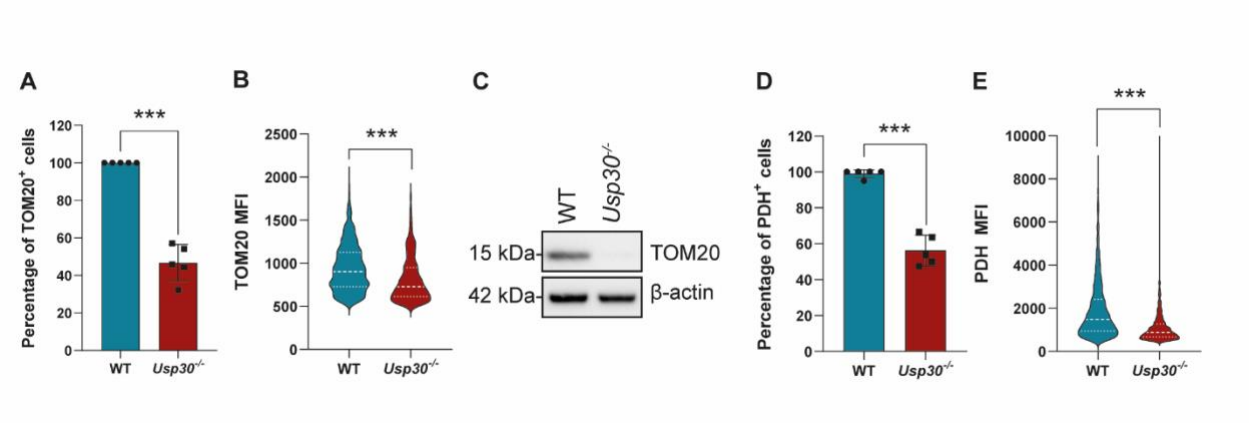

Fig. S2. TOM20 and PDH expression in WT and *Usp30*$^{-/-}$ CTLs.

(A to B) Quantitation of day 5 CTLs expressing (A) TOM20 and (B) TOM20 MFI by immunofluorescence (>65 cells per genotype in each independent repeat). (C) Immunoblot showing TOM20 protein expression in day 5 WT and *Usp30*$^{-/-}$ (KO) CTLs. (D to E) Quantitation of day 5 CTLs expressing (D) PDH and (E) PDH MFI by immunofluorescence (>60 cells per genotype in each repeat). Error bars (A, D) show mean values ±SD of technical replicates in one representative experiment. ***=P<0.001 (two-tailed unpaired Student's *t* test). Dashed lines, median; dotted lines, quartiles in (B, E). All data representative of at least three independent biological replicates.

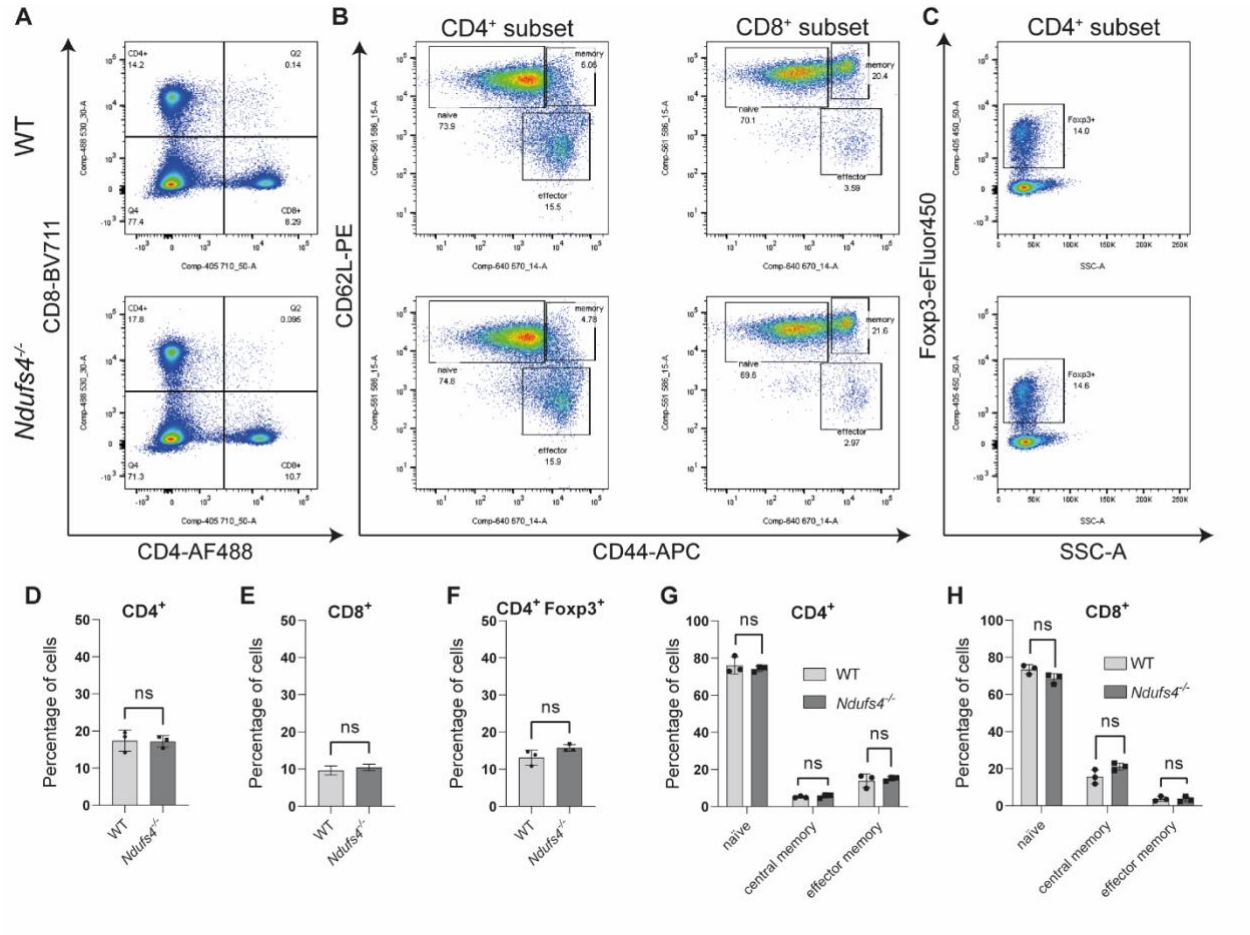

Fig. S3. Analysis of OXPHOS deficiency in splenocytes and CTL killing.

(A to C) WT and *Ndufs4*$^{-/-}$ splenocytes: (A) CD4^{+}/CD8^{+} ratio, (B) CD4^{+} and CD8^{+} naïve (CD62L^{hi}, CD44^{lo}), central memory (CD62L^{hi}, CD44^{hi}) and effector memory (CD62L^{lo}, CD44^{hi}) T cell subsets, (C) regulatory T cells (CD4^{+}, Foxp3^{+}). (D to H) Quantitation of (D) CD4^{+}, (E) CD8^{+}, (F) regulatory T cells, (G) CD4^{+} subsets and (H) CD8^{+} subsets (naïve, central memory, and effector memory). Plots show the average of three biological replicates ±SD. ns= not significant (two-tailed paired Student's *t* test).

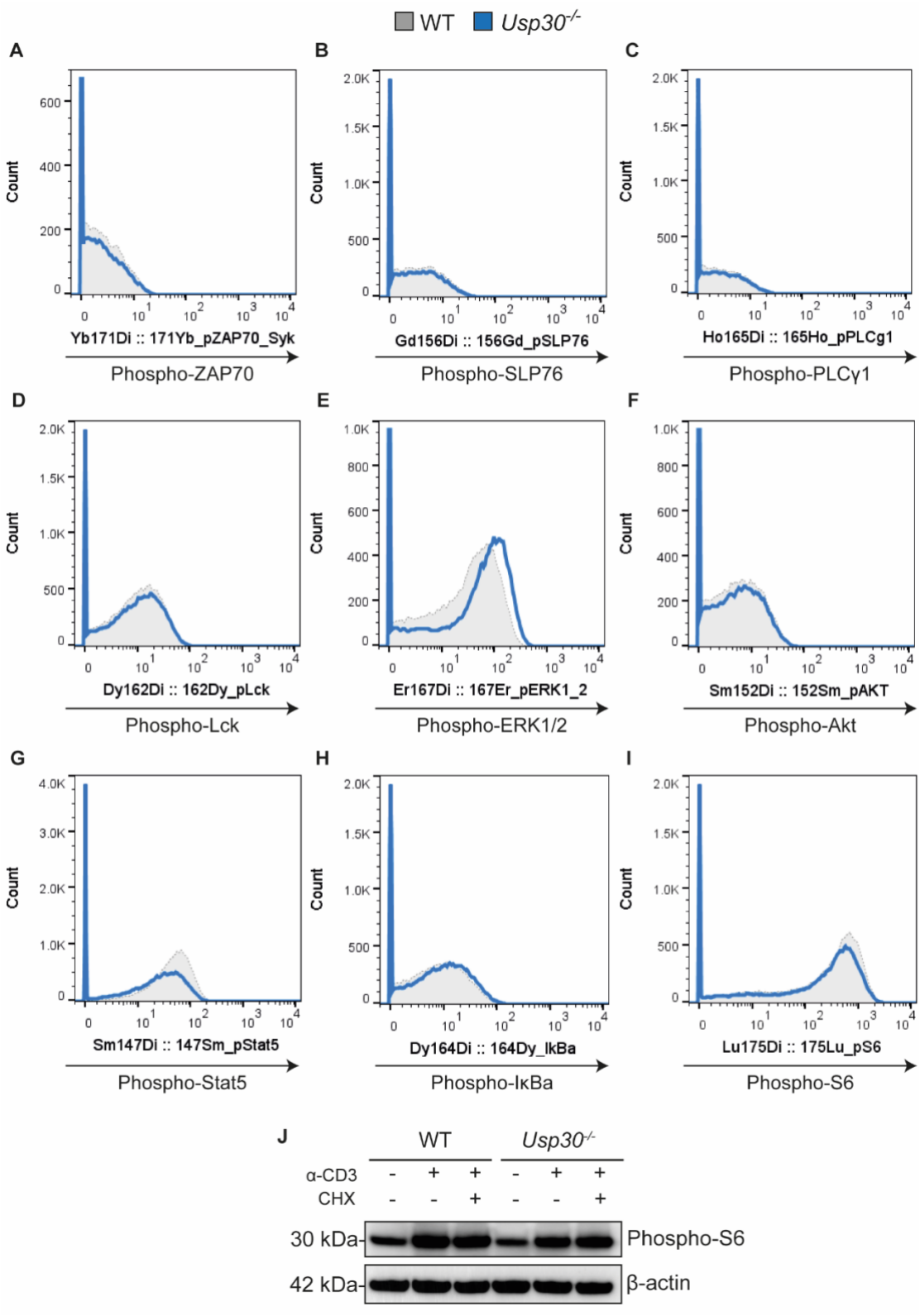

Fig. S4. Proximal and distal TCR signaling is not affected by mitochondrial depletion.

(A to I) TCR signal transduction in anti-CD3-stimulated WT and *Usp30*$^{-/-}$ (KO) CTLs (TCR activated, 1 hour). Phosphorylation of distal and proximal markers was measured via mass cytometry (CyTOF). Histograms showing fluorescence intensity for (A) pZAP70, (B) pSLP76, (C) pPLCγ1, (D) pLCK, (E) pERK1/2, (F) pAKT, (G) pSTAT5, (H) pIκBα, and (I) pS6. (J) Immunoblot showing phosphorylation of the mTOR target S6 in day 5 WT and *Usp30*$^{-/-}$ (KO) CTLs with TCR activation via anti-CD3 stimulation (4.5 hours), and/or cytosolic protein synthesis inhibited by cycloheximide (CHX). S6 phosphorylation increases in both WT and *Usp30*$^{-/-}$ (KO) CTLs upon TCR stimulation. Data representative of at least two independent biological replicates.

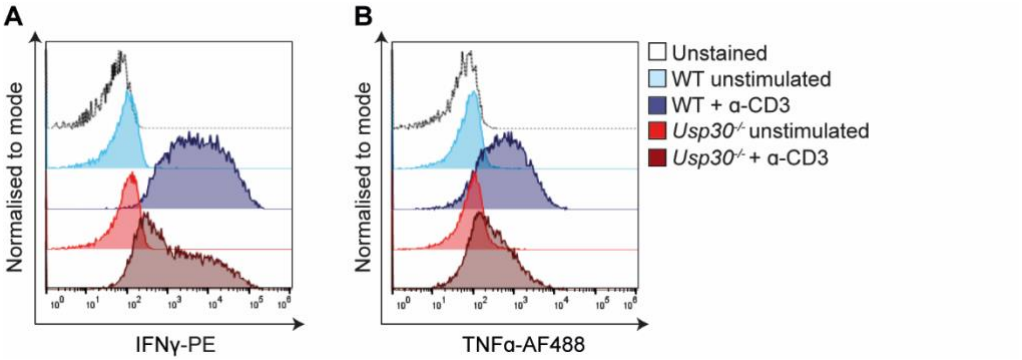

Fig. S5. Cytokine production is impaired in mitochondria-depleted CTLs.

IFNγ (A) and TNFα (B) cytokine production in day 5 WT and *Usp30*$^{-/-}$ (KO) CTLs before and after 4.5 hours anti-CD3 stimulation (TCR activation). Data representative of at least three independent biological replicates.

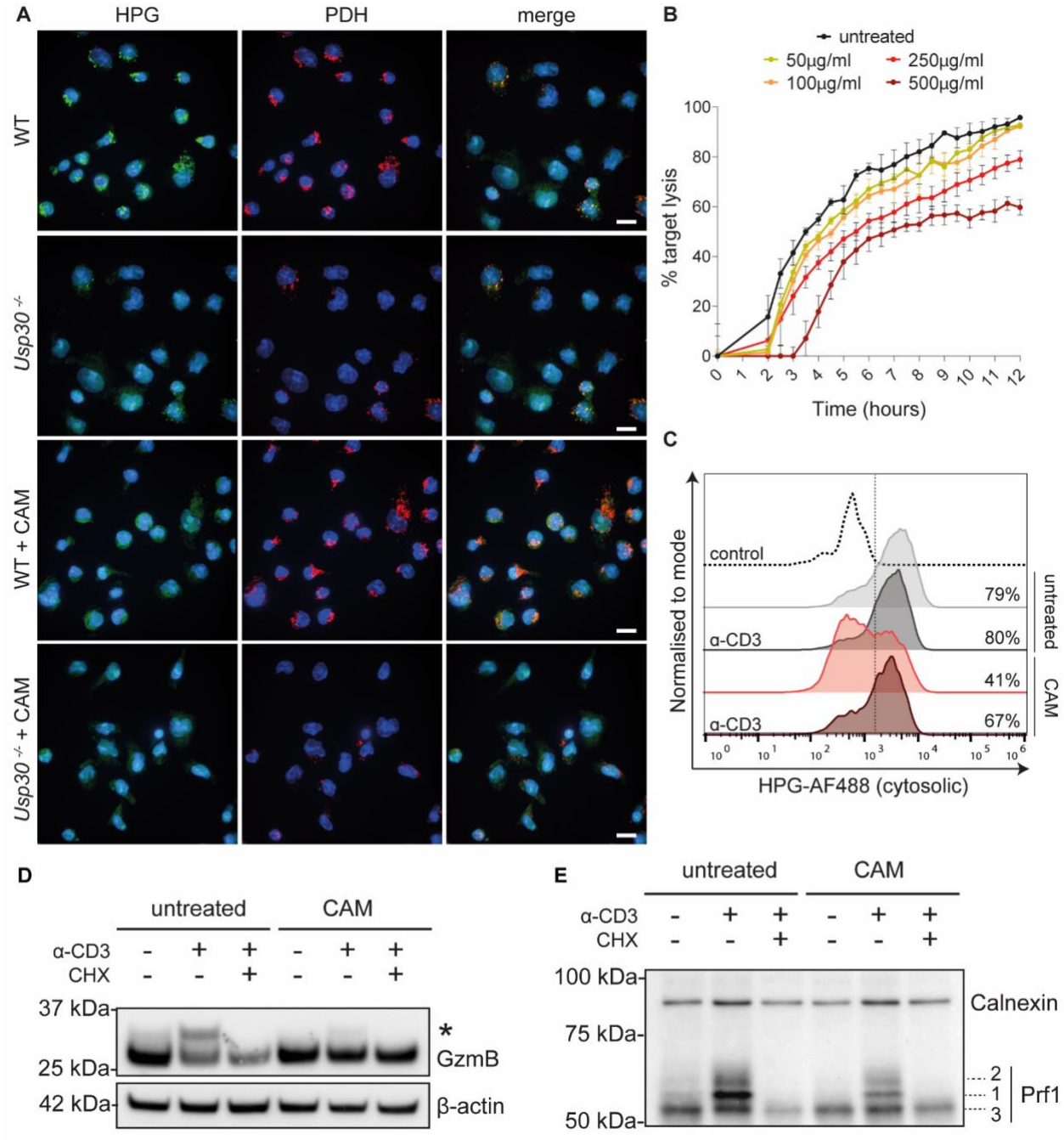

Fig. S6. Chloramphenicol treatment inhibits mitochondrial translation and T cell killing.

(A) Mitochondrial translation visualized by HPG-AF488 incorporation (green) into mitochondria (PDH, red) in day 5 WT and *Usp30*$^{-/-}$ (KO) CTLs treated with cycloheximide (to inhibit cytosolic translation). CTLs were treated where indicated with chloramphenicol (CAM) an inhibitor of mitochondrial translation. Scale bars=10 µm. (B) Long-term (12 hours) killing assay using day 5 WT CTLs (CTL-to-target ratio, 1:1) showing percentage target lysis with increasing concentrations of CAM. Error bars show mean values ±SD of technical replicates

in one representative experiment. (C) HPG-AF488 incorporation into day 5 WT CTLs treated for 1 hour with chloramphenicol (CAM) to inhibit mitochondrial translation or CHX to inhibit cytosolic translation (control), stimulated with anti-CD3 (TCR) where shown. Immunoblots showing (D) granzyme B (GzmB) and (E) perforin (Prf1) in day 5 WT CTLs treated with chloramphenicol (CAM), and/or stimulated via TCR activation (anti-CD3) as indicated for 4 hours. Newly synthesized granzyme B indicated by (*). Immature (1), intermediate (2), and mature (3) forms of perforin are indicated. All data representative of at least three independent biological replicates.

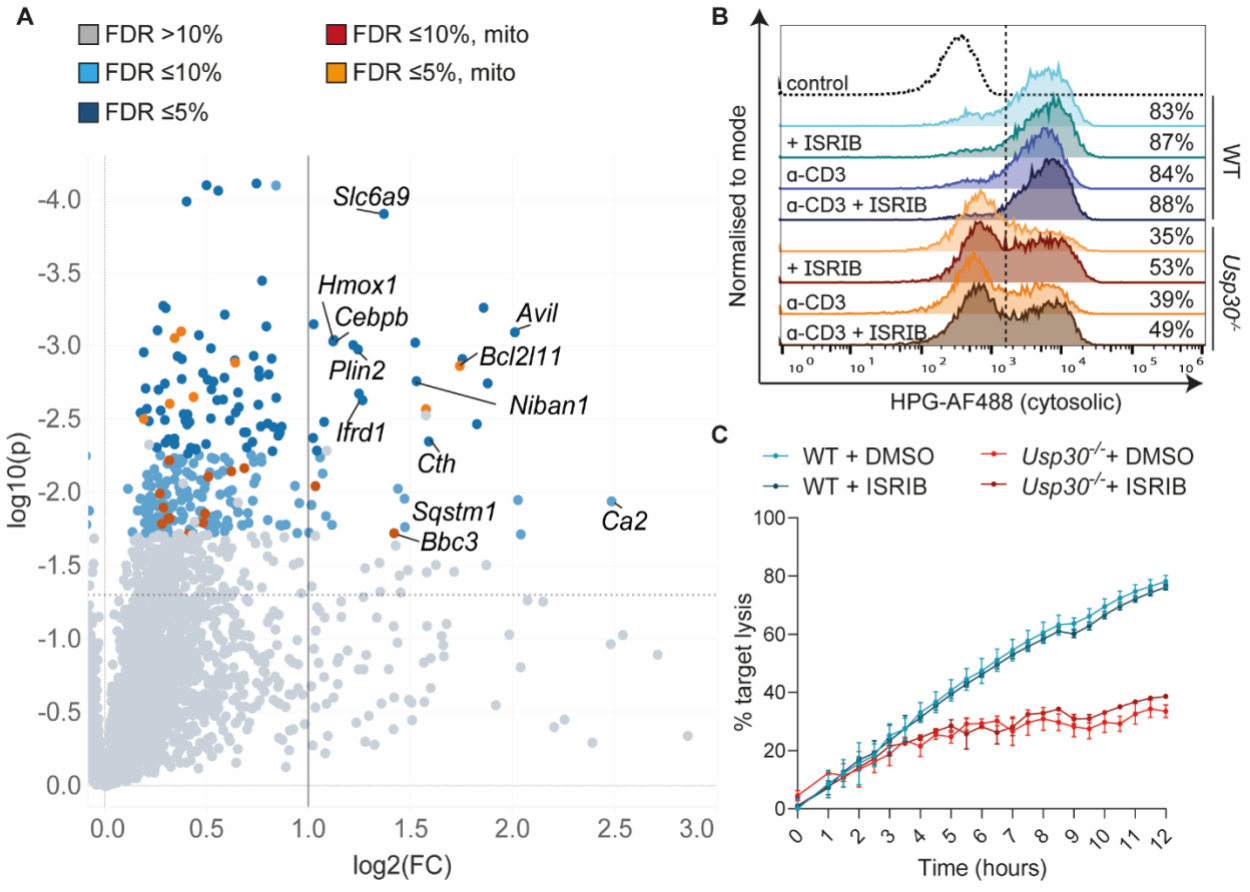

Fig. S7. ISR inhibition is not sufficient to restore translation nor cytotoxicity in *Usp30*$^{-/-}$ CTLs.

(A) Volcano plot of upregulated proteins in day 5 *Usp30*$^{-/-}$ (KO) CTLs compared to WT. Vertical bar denotes log2(FC)=1 and horizontal bar corresponds to the uncorrected *P*=0.05 threshold. Colored dots show hits within the 5% and 10% false discovery rate (FDR) range. GOCC-defined mitochondrial proteins are highlighted according to FDR. Proteins indicating upregulation of the integrated stress response (ISR) are labeled by gene name. (B) HPG-AF488 incorporation in day 5 WT and *Usp30*$^{-/-}$ (KO) CTLs treated with 100 nM ISR inhibitor (ISRIB) (1 hour). TCR activated via anti-CD3 stimulation. Control sample was treated with cycloheximide (CHX) to inhibit cytosolic protein synthesis. (C) Long-term killing assay (CTL to target ratio, 1:1) showing percentage of target lysis with day 5 WT and *Usp30*$^{-/-}$ CTLs treated with 100 nM ISR inhibitor (ISRIB). Error bars show mean values ±SD of technical replicates

in one representative experiment. All data representative of at least three independent biological replicates.

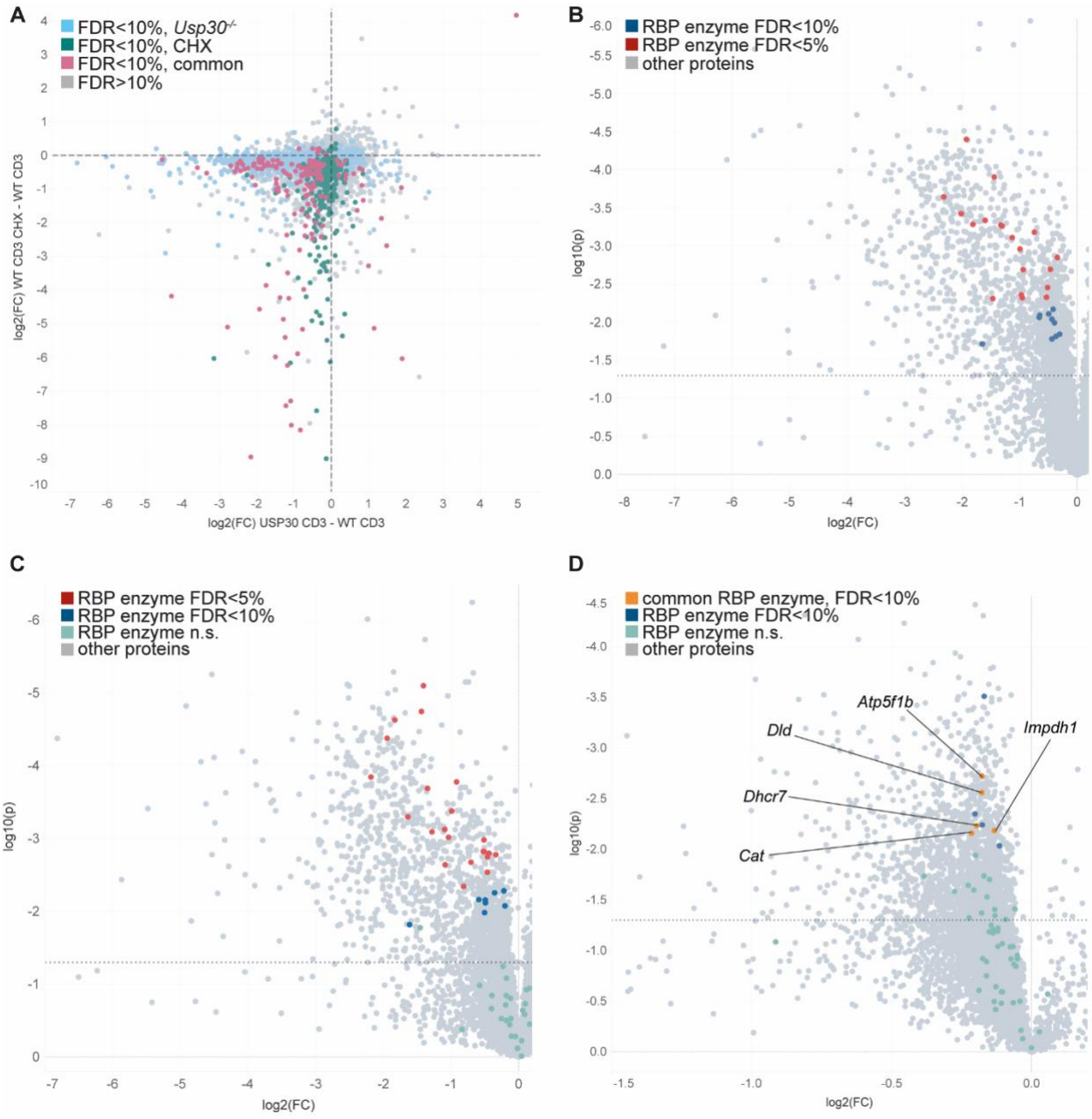

Fig. S8. RNA-binding metabolic enzymes show altered expression in *Usp30*$^{-/-}$ (KO) and doxycycline-treated CTLs.

(A) Proteomes of stimulated (4 hours anti-CD3) day 5 CTLs from *Usp30*$^{-/-}$ (KO) CTLs compared with WT CTLs, and WT CTLs in which cytosolic protein synthesis was inhibited by CHX compared with untreated CTLs. Comparison of effect sizes emphasizes a selective downregulation of protein synthesis in KO CTLs, with only partial overlap with effects of CHX treatment. Dotted lines correspond to $\log_2(FC)=0$. Colored dots show proteins within the 10% false discovery rate (FDR) in the *Usp30*$^{-/-}$ (KO) vs WT dataset (light blue) and in the CHX vs

untreated dataset (green). Magenta-labeled dots indicate proteins within the 10% FDR common to both datasets. (B-C) Volcano plots of downregulated proteins in (B) unstimulated, and (C) TCR-activated day 5 *Usp30*$^{-/-}$ (KO) CTLs compared to day 5 WT. Colored dots show metabolic enzymes moonlighting as RNA-binding proteins (RBP) within the 5% (red) and 10% (blue) FDR range. (D) Volcano plot of downregulated proteins in day 5 CTLs after short-term (4 hours) treatment with doxycycline. Colored dots show enzymes moonlighting as RBP within the 10% FDR range (blue) and RBP enzymes within the 10% FDR showing downregulated expression in both *Usp30*$^{-/-}$ (KO) and doxycycline-treated CTLs (orange). Non-significant (n.s.) RBPs are colored in light green in (C, D). Highlighted proteins referred to by gene name in (D). Horizontal bar: uncorrected P=0.05. All data representative of four independent biological replicates.

Table S1. Mass spectrometry of WT and KO CTLs (separate file)

Proteomics data including gene and protein name, protein description, GOBP/GOMF/GOCC/KEGG terms, mean protein copy number, fold change (FC), p-value (two-tailed paired Student's *t* test) and false discovery rate (FDR, Benjamini–Hochberg method) for day 5 WT and *Usp30*$^{-/-}$ (KO) CTLs.

Table S2. Mass spectrometry of TCR-stimulated WT and KO CTLs (separate file)

Proteomics data including gene and protein name, protein description, GOBP/GOMF/GOCC/KEGG terms, mean protein copy number, fold change (FC), *P*-value (two-tailed paired Student's *t* test) and false discovery rate (FDR, Benjamini–Hochberg method) for day 5 WT and *Usp30*$^{-/-}$ (KO) CTLs after 4.5 hours of anti-CD3-mediated stimulation mimicking TCR activation.

Table S3. Mass spectrometry of TCR-stimulated, CHX-treated WT CTLs (separate file)

Proteomics data including gene and protein name, protein description, GOBP/GOMF/GOCC/KEGG terms, mean protein copy number, fold change (FC), p-value (two-tailed paired Student's *t* test) and false discovery rate (FDR, Benjamini–Hochberg method) for WT CTLs after 4.5 hours of anti-CD3-mediated stimulation mimicking TCR activation. Day 5 CTLs were either left untreated ("WT stimulated") or treated with 100 μg/ml cycloheximide ("WT stimulated + CHX") (4.5 hours).

Table S4. Mass spectrometry of DOX-treated WT CTLs (separate file)

Proteomics data including gene and protein name, protein description, GOBP/GOMF/GOCC/KEGG terms, mean protein copy number, fold change (FC), *P*-value (two-tailed paired Student's *t* test) and false discovery rate (FDR, Benjamini–Hochberg method) for day 5 WT CTLs either left untreated ("WT untreated") or treated with 10 μg/ml doxycycline ("WT + DOX") (4 hours).

Table S5. Table of reagents (see below)

Movie S1. Mitophagy in WT CTLs (separate file)

mt-Keima signal in day 5 WT CTLs migrating on ICAM-1-coated dishes. Green=mitochondria (excitation=488nm); red=mitolysosomes (excitation=561 nm). CTLs imaged for 5 min at 37ºC using a 63 X objective.

Movie S2. Mitophagy in KO CTLs (separate file)

mt-Keima signal in day 5 *Usp30*$^{-/-}$ (KO) CTLs migrating on ICAM-1-coated dishes. Green=mitochondria (excitation=488nm); red=mitolysosomes (excitation=561nm). CTLs imaged for 5 min at 37ºC using a 63 X objective.

Movie S3. WT CTL migration (separate file)

Migration of day 5 WT CTLs on ICAM-1-coated dishes. CTLs nucleofected with Lifeact-mApple to visualize F-actin and stained with Hoechst to label nuclei. CTLs imaged for min at 37ºC using a 63 X objective.

Movie S4. KO CTL migration (separate file)

Migration of day 5 *Usp30*$^{-/-}$ (KO) CTLs on ICAM-1-coated dishes. CTLs nucleofected with Lifeact-mApple to visualize F-actin and stained with Hoechst to label nuclei. CTLs imaged for 5 min at 37ºC using a 63 X objective.

Table S5. Table of reagents

Antibodies

Target	Host	Clone	Fluor	Company	Cat #	RRID	Final conc. /dilution
Mouse CD3ε	Hamster	500A2	none	ThermoFisher	16-0033	AB_842782	0.5-2 µg/ml
Mouse CD3ε	Hamster	145-2C11	none	BDBiosciences	553058	AB-394591	1 µg/ml
Mouse CD28	Hamster	37.51	none	ThermoFisher	16-0281	AB_468921	1 µg/ml
Mouse CD8a	Rat	53-6.7	BV711	Biolegend	100747	AB_2562100	1 µg/ml (Facs)
Mouse CD8a	Rat	53-6.7	APC	Biolegend	100712	AB_312751	1 µg/ml (Facs)
Mouse CD8a	Rat	53-6.7	AF488	ThermoFisher	53-0081	AB_469896	5 µg/ml (IF)
Mouse LAMP1	Rat	1D4B	PE	ThermoFisher	12-1071	AB_657555	2 µg/ml (Facs)
Mouse LAMP1	Rat	1DB4	none	DSHB	1DB4	AB_2134500	1:2 (IF)
γ-tubulin	Rabbit	polyclonal	none	Sigma	T5192	AB_261690	1:1000
β-actin	Mouse	AC-15	none	Sigma	A1978	AB_476744	1:5000
Calnexin	Rabbit	Polyclonal	none	Sigma	C4731	AB_476845	1:5000
Granzyme B	Rabbit	Polyclonal	none	Abcam	ab4059	AB_304251	1:500
Mouse perforin	Rat	CB5.4	none	Enzo	ALX-804057	AB_2052202	1:500
TOM20	Mouse	4F3	none	Abcam	ab56783	AB_945896	4 µg/ml (WB) 10 µg/ml (IF)
PDH	Mouse	9H9AF5	none	Abcam	ab110330	AB_10858459	1 µg/ml (IF)
pS6 (S240/244)	Rabbit	D68F8	none	Cell Signaling	5364S	AB_10694233	1:500
Mouse IFNγ	Rat	XMG1.2	PE	BioLegend	505808	AB_315402	1 µg/ml
Mouse TNFα	Rat	MP6XT22	AF488	BioLegend	506313	AB_493328	1 µg/ml
Rabbit IgG	Goat	polyclonal	HRP	ThermoFisher	A16110	AB_2534782	1:10,000
Mouse IgG	Goat	polyclonal	HRP	ThermoFisher	A16078	AB_2534751	1:10,000
Rat IgG	Goat	polyclonal	HRP	ThermoFisher	31470	AB_228356	1:10,000
Mouse IgG	Goat	polyclonal	AF546	ThermoFisher	A-11030	AB_144695	5 µg/ml (IF)
Rabbit IgG	Donkey	polyclonal	AF647	ThermoFisher	A-31573	AB_2536183	5 µg/ml (IF)
Hamster IgG	Goat	polyclonal	none	ThermoFisher	31115	AB_394591	50 µg/ml (Facs)

Dyes

Reagent	Supplier	Cat #	Final conc
Hoechst 33342	ThermoFisher	H3570	1:50,000
Zombie Yellow (Viability)	BioLegend	423103	1:400
Zombie Violet (Viability)	BioLegend	423114	1:400
Zombie Aqua	BioLegend	423102	1:400
MitoTracker Green	ThermoFisher	M7514	100 nM
TMRE	Abcam	ab113852	100 nM
INDO-1	ThermoFisher	I1223	1 µM

Media and cell culture

Reagent	Supplier	Cat #	Final conc
RPMI 1640	ThermoFisher	21875	
DMEM	ThermoFisher	41966	
RPMI no methionine	ThermoFisher	A1451701	
CO2-independent media	ThermoFisher	18045-054	
Phenol red free RPMI	Gibco	32404-014	
L-Glutamine	Sigma	G7513	2 mM
Sodium pyruvate	Sigma	11360070	1 mM
Penicillin & Streptomycin	ThermoFisher	P0781	100 U/ml & 1 mg/ml
β-mercaptoethanol	ThermoFisher	31350010	50 µM
Foetal bovine serum (FBS)	LabTech, FBS-Sa		10%
Recombinant murine IL-2	Peprotech	212-12	100 U/ml
Puromycin (selection)	ThermoFisher	A11138	1 µg/ml

Mice

Strain	Background	Supplier	RRID
C57/BL6N/WTSI (WT)	C57/BL6N	Wellcome Trust Sanger Institute	SCR_006158
C57BL/6N-Usp30$^{tm2b(EUCOMM)Hmgu}$/Wtsi	C57/BL6N	Wellcome Trust Sanger Institute	IMSR_EM:09833

Cell lines

Cell line	Species/origin	Supplier	RRID
P815	Mouse mastocytoma	Basel Institute for Immunology	CVCL_2154

Inhibitors

Reagent	Supplier	Cat #	Final conc
Doxycycline	Merck	D9891	10 μg/ml
Chloramphenicol	Sigma	R4408	50-500 μg/ml
ISRIB	Sigma	SML0843	100 nM
FCCP	Sigma	C2920	1 μM
Oligomycin	Sigma	75351	1 μM
Rotenone	Sigma	R8875	0.5 μM
Antimycin A	Sigma	A8674	0.5 μM
Cycloheximide	Sigma	C4859	100 μg/ml

CD8+ isolation and Nucleofection reagents

Reagent	Supplier	Cat #
CD8a$^+$ T Cell Isolation Kit	Miltenyi	130-104-075
P3 Primary Cell Nucleofector Kit	Lonza	V4XP-3024
Mouse T Cell Nucleofector Kit	Lonza	VZB-1001

qPCR reagents

Reagent	Supplier	Cat #
RNeasy mini kit	Qiagen	74104
QIAshredder columns	Qiagen	79654
Accuscript cDNA synthesis kit	Agilent	200820
TaqMan gene expression mastermix	ThermoFisher	4369016
TaqMan gene expression assay	ThermoFisher	4331182
Mouse granzyme B qPCR probe	ThermoFisher	Mm00442837_m1
Mouse perforin qPCR probe	ThermoFisher	Mm00812512_m1
Mouse TATA-binding protein (Tbp) qPCR probe	ThermoFisher	Mm01277042_m1

HPG protein synthesis reagents

Reagent	Supplier	Cat #
Click-iT HPG Alexa Fluor 488 Protein Synthesis Assay	ThermoFisher	C10428
Click-IT L-homoproparglycine (HPG)	ThermoFisher	C10186

Seahorse reagents

Reagent	Supplier	Cat #
Seahorse XF Cell Mito Stress Test Kit	Agilent	103015-100
Seahorse XFe96 FluxPak cartridge	Agilent	102416-100
Seahorse XF Calibrant solution	Agilent	103059-000
Cell-Tak	Corning	354240
DMEM for Seahorse assay	Sigma	D5030
Glucose for Seahorse assay	ThermoFisher	A2494001

Other reagents

Reagent	Supplier	Cat #

Recombinant mouse ICAM-1/CD45 Fc	R&D Systems	796-IC
Triton X-100	Sigma	T8787
Saponin	Sigma	S7900
Paraformaldehyde (PFA)	Electron Microscopy Sciences	15710-S
Glutaraldehyde	Agar Scientific	AGR1020
Bovine Serum Albumin (BSA)	Sigma	A7906
ProLong Diamond Antifade Mounting medium	Life Technologies	P36961
Foxp3 Transcription Factor Staining Buffer Set	ThermoFisher	00-5523-00
ECL Prime Western Blotting Detection Reagent	GE Healthcare	RPN2232
ATP Determination Kit	ThermoFisher	A22066
CytoTox 96 Non-Radioactive Cytotoxicity Assay	Promega	G1780